Atomic Spectroscopy

Review

Advances in Laser-induced Breakdown Spectroscopy for Real-time Monitoring

Yun Tang,* Enxin Guo, Zeen Yang, Sheng Wang, and Jiale Liao

Hunan Province Key Laboratory of Intelligent Sensors and Advanced Sensor Materials, College of Physics and Electronic Science, Hunan University of Science and Technology, Xiangtan 411100, P. R. China

Received: *December 02, 2025;* ***Revised:*** *January 23, 2026;* ***Accepted:*** *January 27, 2026;* ***Available online:*** *January 27, 2026.*

DOI: 10.46770/AS.2025.283

ABSTRACT: Laser-Induced Breakdown Spectroscopy (LIBS)technology, a type of atomic emission spectrometry analysis that utilizes a laser as an excitation source, has undergone rapid development in recent years owing to its rapid, in-situ, multi-element detection capabilities and minimal sample preparation. Although its sensitivity is generally lower than that of inductively coupled plasma mass spectrometry (ICP-MS) and some other techniques, LIBS—by virtue of its deployment flexibility, portability, and the foregoing attributes—is better suited to online monitoring. This work summarizes the latest research progress of LIBS in the field of real-time monitoring and provides a comprehensive comparative analysis of the strengths and weaknesses of LIBS relative to XRF, ICP-MS, and other related techniques, specifically focusing on industrial raw material/product quality control during manufacturing, in situ elemental analysis during laser processing, and environmental pollutant emissions tracking. Across these applications, LIBS exhibits variable detection stability and sensitivity: in industrial settings, relative standard deviations (RSDs) typically remain below 15% (with minor elements reaching 15–30%), while detection limits (LODs) predominantly range at ppm levels (with limited ppb-level achievements). Environmental monitoring shows RSDs heavily dependent on instrumentation and field conditions, with reported LODs spanning ng/m³ to mg/m³ (air pollutants), μg/L to mg/L (water quality), and mg/kg (soil analysis). This work also explores the practical challenges encountered during the implementation of LIBS across various domains. In the industrial sector, the primary obstacles involve suboptimal detection accuracy and stability, stemming from high solid-surface complexity, the difficulties of liquid metal analysis, contamination of metallurgical molds, and harsh operating environments. Within the field of laser processing, the challenges mainly arise from the instability of the welding molten pool and the ambiguity in defining thresholds for determining the extent of machining. Conversely, environmental monitoring is primarily constrained by relatively low sensitivity when analyzing gaseous and liquid states. Finally, targeted solutions corresponding to the specific technical challenges in each field are proposed. Future developments in signal enhancement are anticipated to overcome current technical constraints, enabling robust high-sensitivity, multi-element detection in complex sample systems.

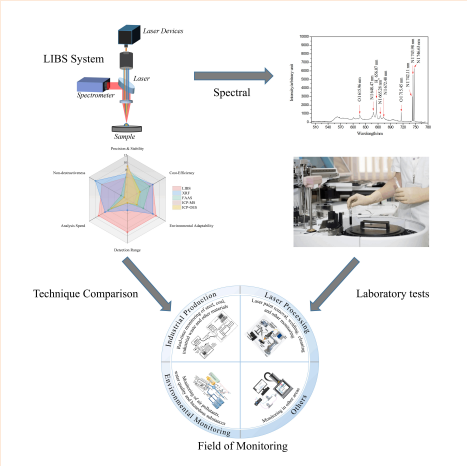

INTRODUCTION

Laser-induced breakdown spectroscopy (LIBS) is an analytical technique that employs a focused laser pulse to generate plasma on a sample surface, enabling compositional analysis through the spectral emission of the plasma. Upon irradiation, the laser pulse ablates a minute portion of the sample, vaporizing and ionizing it to form a transient, high-temperature, high-density plasma. The emitted light is then collected by a spectrometer and resolved into discrete spectral lines, each corresponding to characteristic wavelengths of the constituent elements. This spectral information allows both qualitative and quantitative elemental analysis of the sample.

Compared with established elemental analysis techniques—such as X-ray fluorescence (XRF)[1], inductively coupled plasma

mass spectrometry (ICP-MS)[2], inductively coupled plasma optical emission spectrometry (ICP-OES)[3], and flame Atomic Absorption Spectrometry (FAAS)[4]—LIBS offers several distinctive advantages. It provides rapid response, supports multi-element detection, enables in situ and real-time analysis, and eliminates the need for sample preparation.

Real-time monitoring is indispensable in numerous industrial and environmental contexts. From manufacturing process control and environmental pollution assessment to applications in food safety and medical diagnostics, the ability to acquire fast and precise data facilitates immediate situational awareness and supports prompt decision-making and intervention. In industrial production in particular, the availability of accurate real-time data is integral to enhancing productivity, ensuring quality control, maintaining operational safety, and reducing costs[5-7].

Given its capability for in situ, real-time elemental analysis, LIBS has been increasingly adopted for monitoring in industrial and environmental settings[8–12]. The structure of this review is organized as follows: Section 2 provides a comparative analysis of the advantages and limitations of LIBS relative to other elemental analysis techniques, such as FAAS and XRF, specifically under real-time monitoring conditions. Subsequently, Section 3 to 6 survey the progress of LIBS in real-time monitoring across various fields. Specifically, Section 3 focuses on industrial production, emphasizing real-time quality control in sectors such as coal and steel, while evaluating its contributions to production efficiency, quality assurance, and safety maintenance. Section 4 discusses the implementation of LIBS for real-time monitoring during laser processing to enhance machining precision and efficiency. Section 5 presents case studies in environmental monitoring, analyzing the strengths and challenges of LIBS when addressing rapidly changing environmental conditions. Given the continuous expansion of LIBS applications, Section 6 explores emerging fields, including fundamental and specialized manufacturing processes as well as medical diagnostics, providing a comprehensive discussion and comparison. Finally, Section 7 concludes by reviewing the current application status across these domains and offering perspectives on future developmental trends. Particular attention is given to identifying technical bottlenecks in real-time monitoring and proposing potential solutions or research hotspots to provide a roadmap for the further advancement of LIBS technology.

COMPARATIVE ANALYSIS OF LIBS AND OTHER ELEMENTAL ANALYSIS TECHNIQUES

Compared with LIBS, techniques such as FAAS (1950s–1960s), XRF (1960s), ICP-OES (1970s), and ICP-MS (1980s) emerged much earlier, and the advantages of most of these methods became established over time and are well demonstrated under routine laboratory conditions. Although each technique has its own strengths (*e.g.*, the high sensitivity of ICP-OES and the non-destructive nature of XRF), the range of elemental-analysis methods that are truly suitable for on-site, real-time monitoring has remained extremely limited amid the growth of industrial manufacturing, medical services, and geological exploration.

Numerous studies[13-17] have comparatively analyzed LIBS, FAAS, ICP-OES, ICP-MS, and XRF in terms of principles and performance. Accordingly, this article does not provide a detailed comparison of fundamental mechanisms; instead, it offers a concise overview of the strengths and limitations of these techniques and explains why LIBS is more widely applicable to real-time monitoring.

Both GF AAS and FAAS are types of AAS, with their typical feature being single-element analysis. GF AAS offers high sensitivity but is limited in precision, while FAAS provides better precision but lower sensitivity. Both techniques require sample digestion and sequentially switching between elemental channels, which makes multi-element detection infeasible and results in slower measurement speeds, making them unsuitable for rapid in-situ analysis. ICP-MS and ICP-OES are known for their superior sensitivity, with ICP-MS generally outperforming ICP-OES. However, both techniques involve highly complex instrumentation, such as the need for high vacuum systems in ICP-MS and precise gas flow management in ICP-OES, along with high operational costs. These stringent instrumental requirements limit their flexibility in real-time, on-site monitoring applications, as real-time monitoring in industrial or environmental fields demands not only high sensitivity but also rapid response, portability, operational flexibility, and cost-effectiveness. XRF, while non-destructive, is not well-suited for real-time monitoring due to its stringent instrumental requirements, such as the need for stable energy sources and precise sample positioning. Furthermore, XRF has poor sensitivity to low-atomic-number elements like hydrogen (H) and lithium (Li), preventing it from meeting the needs of rapid, in-situ, multi-element analysis.

A schematic diagram of a typical LIBS system is presented in Fig. 1.[18] The system consists of a laser source, spectrometer, optical fiber, CCD detector, and data acquisition module. In some LIBS systems, the laser focusing head can be routed via optical fiber and positioned tens of meters away, allowing the laser spot to "scan" the surfaces of conveyor belts, ducts, or melt pools[19]; other LIBS instruments are compact, relatively lightweight, and easier to install than alternative equipment[20]. Taken together, these attributes underscore the flexibility and portability of LIBS instrumentation. These features highlight the advantages of LIBS systems in terms of flexibility and portability compared to other elemental analysis techniques. Due to its significant benefits in

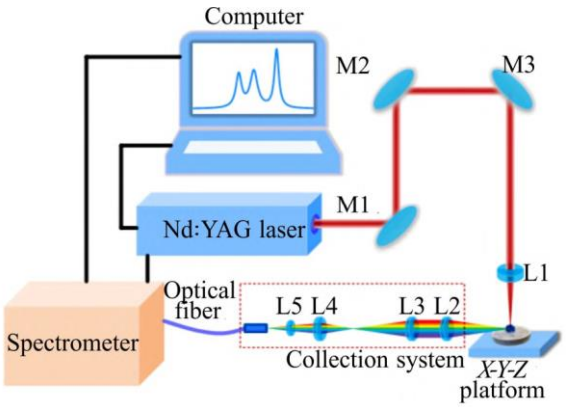

Fig. 1 A typical LIBS analytical system (adapted from [18])

real-time monitoring, the technology has rapidly developed in recent years and its application areas continue to expand.[16,21].

Despite the inherent advantages of LIBS for in situ monitoring, the technique is subject to several constraints. Specifically, the detection precision of LIBS is generally inferior to that of ICP-MS and ICP-OES. Furthermore, its quantitative stability is lower than that of established elemental analysis techniques such as ICP-MS and XRF. Most critically, LIBS analysis is highly susceptible to matrix effects, which can induce non-linear response ranges and subsequently compromise analytical accuracy. The matrix effect refers to the phenomenon where variations in the physical properties (such as hardness and reflectivity) or chemical composition (major constituent content) of a sample lead to differing spectral intensities for the same concentration of a target element. This effect remains a significant challenge for LIBS across numerous application scenarios. Consequently, LIBS may not be suitable for real-time monitoring scenarios that demand extreme sensitivity or exceptional stability, such as precision instrument manufacturing. However, as researchers extend LIBS applications into increasingly diverse fields and continue to enhance instrumental precision and stability by mitigating matrix effects, LIBS is poised to become one of the most promising and practical analytical tools in the realm of real-time monitoring. Table S1 provides a comprehensive comparison of LIBS, AAS, XRF, ICP-MS, and ICP-OES across various parameters essential for real-time applications.

Section 2 primarily benchmarks the advantages and limitations of LIBS against techniques such as AAS, XRF, and ICP-MS within the context of real-time monitoring. Overall, LIBS exhibits a superior balance of attributes, fueling its rapid proliferation across various sectors. Sections 3 through 7 present the recent advancements in real-time monitoring within their respective fields while addressing current shortcomings. Finally, the review concludes with a summary and a perspective on the future trajectory of LIBS technology.

ONLINE MONITORING OF INDUSTRIAL PROCESSES

Industrial development has become an essential component of modern society. In general, industrial production encompasses several key stages: raw material acquisition and preparation, processing and manufacturing, assembly and production, quality control and monitoring, as well as packaging and transportation. These stages must operate in coordination to achieve effective production management and high-quality outputs, which in turn drive economic growth[22].

This section is systematically organized into six sub-sections. The first four primarily focus on the real-time monitoring of critical raw materials during classification and quantitative analysis using LIBS technology, while Section 5 provides a comprehensive review of the real-time monitoring of industrial waste generated during production. The final section provides a comprehensive summary of the topics discussed throughout this chapter. Specifically, Section 1 introduces real-time monitoring for the quantitative analysis and sorting of minerals; by tracking mineral composition in real time, this technology enhances resource recovery rates during mining and provides essential feedback for production lines to improve efficiency—representing a foundational scenario for elemental monitoring in industrial processes. Section 2 then shifts the focus to real-time monitoring for coal quality control and safety during production. As a primary global energy source, real-time monitoring of coal quality is paramount for optimizing combustion efficiency and mitigating pollutant emissions. Section 3 targets the steel production process, which typically involves high-temperature molten states and harsh industrial environments, thereby posing more stringent challenges to the adaptability of real-time LIBS monitoring systems. Building upon these discussions, Section 4 extends the scope to other alloy smelting processes, demonstrating the versatility and adaptability of LIBS across diverse metallurgical systems. Given that various industrial activities frequently generate substantial quantities of hazardous waste residues that adversely impact the environment and ecological health, Section 5 reviews the real-time monitoring of diverse industrial wastes. Finally, the last section provides a systematic summary of the applications discussed in this chapter, examines the challenges faced by LIBS monitoring in industrial production, and proposes several potential solutions.

Real-time Monitoring of Mineral Analysis and Sorting. In 1996, Blacic J. D. and his team[23] reported the use of portable LIBS for real-time rock analysis at Yucca Mountain. Their study confirmed the capability of LIBS for in situ elemental analysis and characterization by successfully examining various rock samples. Additionally, laboratory-based LIBS measurements identified characteristic elemental ratios of manganese oxide minerals along the Yucca Mountain fault, providing a means to differentiate between rock mineral types.

Building on this work, Gaft *et al.*[24] conducted field tests of LIBS for phosphate ore analysis. They reported errors ranging from 0.16% to 0.34% for MgO, FeO, and Al_2O_3. Although the correlation for Al was lower than for the other elements, the field results closely matched laboratory findings, underscoring the system's strength in elemental analysis under field conditions. Subsequently, they evaluated double-pulse LIBS for sulfur detection in minerals under different environmental conditions. Their experiments successfully identified sulfur in both the NIR and UV spectral regions, demonstrating detection limits of 5–10% in the NIR range and approximately 1% in the UV range. Furthermore, they showed that spectral accuracy in the UV region could be enhanced by filling the spectrometer with N_2.[25]

The same research group developed a field-deployable industrial LIBS analyzer for the in situ analysis of diverse minerals, including phosphate, magnesite, copper, and nickel ores. Their findings demonstrated that the data acquired via in situ LIBS analysis were comparable to laboratory-grade results, while the significantly faster response times substantially enhanced process control efficiency. Furthermore, the study benchmarked LIBS against established online techniques such as X-ray Fluorescence (XRF) and Prompt Gamma Neutron Activation Analysis (PGNAA), highlighting that LIBS operates without generating ionizing radiation—thereby mitigating safety risks and circumventing the need for complex radiation safety permits. Compared with conventional laboratory methodologies, in situ LIBS detection provides real-time, continuous online data, facilitating proactive quality monitoring and operational optimization[26].

In a separate study, Death D. L. and coworkers[27] integrated LIBS with Principal Component Analysis (PCA) and Principal Component Regression (PCR) for the rapid online analysis of silicate and various iron ores, yielding robust analytical outcomes. The team further contrasted LIBS with XRF technology, noting that while industrial samples are traditionally processed via laboratory-based XRF—often entailing reporting cycles of up to 48 hours—the primary advantage of LIBS lies in its "immediacy." Collectively, these results underscore the core advantages and application potential of LIBS for online monitoring relative to traditional analytical techniques.

Cheng *et al.*[28] addressed the challenges of sample splashing and sedimentation during slurry flotation by designing a slurry circulation system to improve LIBS reproducibility for online monitoring. Fig. 2 illustrates the LIBS system integrated with this circulation system, while Fig. S1 depicts the slurry sample container. Their system—comprising a laser, plano-convex lens, spectroscope, spectrometer, and host computer—achieved a linear fit coefficient of 0.982 for Fe, a detection limit of 0.075 wt.%, and root mean square error prediction (RMSEP) and average relative error prediction (AREP) values of 0.218 wt.% and 6.96%,

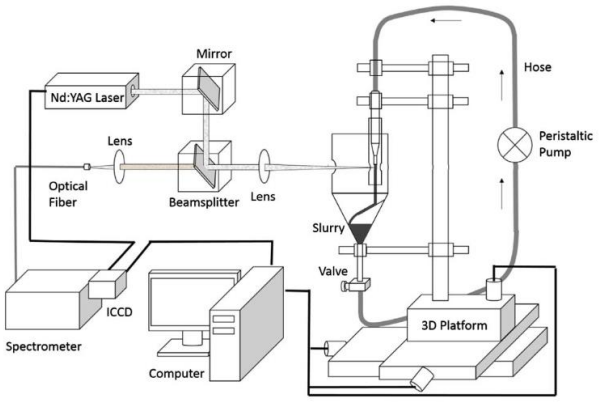

Fig. 2 LIBS system and circulation system for slurry analysis (adapted from [28]).

respectively. These results indicate both high prediction accuracy and detection limits below typical iron content levels in certain ores.

El Haddad *et al.*[29] employed multivariate curve resolution–alternating least squares (MCR-ALS) to analyze LIBS data, effectively deconstructing the spectra of complex mineral mixtures—including feldspar, albite, chlorite, chalcopyrite, and pyrite—to isolate pure mineral profiles for quantitative analysis. The LIBS analytical data exhibited high consistency with Quantitative Mineral Analysis (QMA) results, yielding a root mean square error (RMSE) below 10%.

In 2020, Wójcik *et al.*[30] proposed a scheme integrating handheld LIBS with non-negative tensor factorization (NTF) for the classification of various copper ores. Compared to conventional methods such as support vector machines (SVM), NTF serves as an unsupervised learning approach that extracts pattern-related non-negative latent components from multi-dimensional arrays (tensors), thereby achieving superior classification accuracy. The handheld LIBS instrument utilized in their study is characterized by its compact footprint and high portability, making it uniquely suited for in situ mineral detection in spatially constrained environments, such as underground mines and remote geological sites.

While the aforementioned experiments focused on copper ore classification, the real-time quantitative analysis of copper content in concentrates is equally vital for copper production. Subsequently, Fuentes R. and colleagues[31] adopted a data fusion approach combining LIBS with diffuse reflectance spectroscopy (DRS) to monitor mineral content in copper concentrates in real time, facilitating the optimization of extraction and processing workflows. The study evaluated two integration strategies—low-level data fusion (LLDF) and mid-level data fusion (MLDF)—finding that the latter possessed stronger predictive power than the former, significantly outperforming standalone LIBS or DRS data,

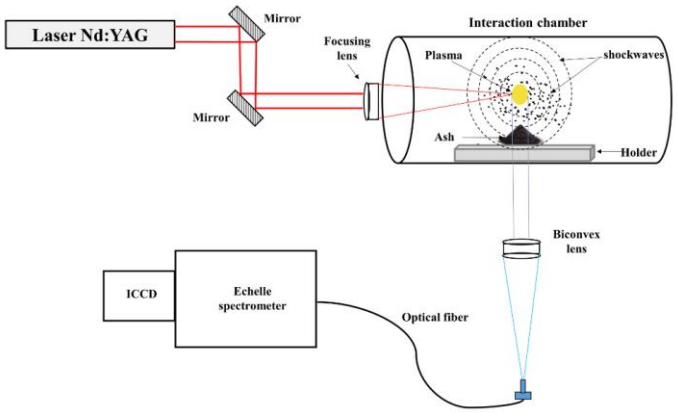

Fig. 3 Experimental setup for laser-induced breakdown spectroscopy (LIBS) for fly ash measurements (adapted from [39]).

with R^2 values ranging from 0.89 to 0.98 across different ores. One year later, Álvarez *et al.*[32] performed quantitative analysis on various copper ores by coupling LIBS with chemometric techniques, including partial least squares regression (PLSR), artificial neural network regression (ANNR), and MCR-ALS. The results indicated that for overall predictive performance across all ore types, the ANNR model outperformed PLSR, which in turn surpassed MCR-ALS. ANNR provided the highest R^2 of 0.986 (for iron oxides) with a root mean square error of prediction (RMSEP) of only 0.334, demonstrating exceptional predictive precision.

Furthermore, Rifai *et al.*[33] utilized LIBS technology developed by ELEMISSION to detect platinum-group element (PGE) ores. They employed a supervised learning algorithm based on principal component analysis (PCA) combined with LIBS data for mineral phase identification. By comparing the multi-phase mineral distribution maps generated by LIBS with scanning electron microscopy-energy dispersive spectroscopy (SEM-EDS) data, they observed excellent data consistency. This validated the efficacy of the LIBS instrument for field-deployable, real-time monitoring and automated mineral phase identification. Similarly, Huang J. and coworkers[34] performed in situ detection and classification of five mineral types—hematite, limonite, shale, granite, and quartz—using LIBS. By optimizing the spectral data through a combination of PCA and back-propagation artificial neural networks (BP-ANN), they achieved a peak recognition accuracy of 100%. Following ten-fold cross-validation, the final identification accuracy remained robust at 93.67%.

Recent research has further enhanced LIBS performance in mineral classification. Li *et al.*[35] incorporated a Cassegrain telescope into the LIBS optical system and applied preprocessing algorithms such as baseline correction and spectral normalization, significantly improving spectral stability and accuracy. Their optimized approach achieved a root mean square error of prediction (RMSEP) of approximately 1.3% for Fe and a mean absolute error (MAE) of 0.91%. Building on this, Chen *et al.*[36] introduced a quantitative analysis method combining Morse wavelet transform with a lightweight convolutional neural network (MsWT-LCNN). This approach yielded an average absolute error of only 0.93% across 121 validation spectra, fully meeting industrial accuracy standards.

Beyond mineral analysis in industrial contexts, LIBS has also become a key tool in volcanic ash research. As early as 2004, studies[37] explored its feasibility for qualitative and quantitative analysis of silicate-rich terrestrial materials under simulated dilute atmospheric conditions. These investigations confirmed that LIBS can deliver stable, efficient, and real-time elemental monitoring even in extreme environments such as high temperature and low pressure, making it well-suited for volcanic ash monitoring.

Further advancements include work by De Giacomo and Taleb [38,39], who evaluated calibration-free LIBS (CF-LIBS) for volcanic ash analysis under both laboratory and simulated volcanic plume conditions. Fig. 3 illustrates their CF-LIBS setup, which operated at laser energies of 100–300 mJ. By measuring the spectral radiance of homogeneous plasmas in local thermodynamic equilibrium, CF-LIBS enabled accurate determination of elemental composition. Their findings showed that major elements such as Si and Al could be quantified with accuracies of 5–10%, validating the method's effectiveness for characterizing volcanic plume emissions in real time.

The aforementioned research achievements demonstrate the broad applicability of LIBS technology across diverse ore compositions and complex geological environments. To provide a more systematic overview of the technical methodologies and practical efficacy of LIBS in the field of real-time mineral monitoring, Table 1 summarizes representative application cases from recent years across three dimensions: the target mineral species, the core analytical methods employed, and the primary research contributions.

Table 1. The contribution of LIBS in real-time monitoring for mineral classification or quantitative analysis in various studies

Minerals	Auxiliary LIBS Technology	Contributions	Refs
Manganese oxide minerals, tuff, medical stone	---	Two distinct prototypes of field-portable LIBS instruments were designed and constructed, demonstrating the feasibility of real-time elemental analysis for rocks encountered during air-core drilling at Yucca Mountain.	23
Phosphate ore	---	LIBS technology has shown high competitive potential in the mineral industry compared to existing online analyzers (e.g., PGNAA).	24
Sulfur ore, copper ore, nickel ore, etc.	Dual-pulse LIBS	A 2-2.5 fold enhancement of sulfur spectral signals was achieved, with a minimum detectable sulfur content of less than 1%.	25
Phosphate ore, magnesium ore, copper ore, nickel ore, etc.	---	A field-portable LIBS industrial analyzer was developed, which offers advantages of real-time continuous measurement and low safety risks compared to conventional laboratory-based LIBS technology, as well as XRF and PGNAA analytical techniques.	26
Iron ore, nickel ore, and phosphate ore	PCA, PCR	PCA and PCR models were employed for multi-element quantitative analysis of iron ore, and phosphorus content in ores was analyzed for the first time by combining LIBS data with PCA.	27
Iron ore slurry	Slurry circulation system	A slurry circulation system was developed, which successfully improved the repeatability of LIBS online monitoring and reduced interference caused by sample splashing, sedimentation, and other issues during ore slurry flotation. Average RSD: Fe 6.96% LOD: Fe 0.075 wt.%	28
Mixed minerals (feldspar, albite, chlorite, chalcopyrite, pyrite, etc.)	MCR-ALS	MCR-ALS was applied for LIBS data analysis. The high consistency (absolute error < 4%) between LIBS data and QMA data verified the advantages of LIBS technology in efficient and accurate identification of mixed minerals.	29
62 types of copper ores (azurite, malachite, chalcopyrite, etc.)	NTF, handheld LIBS	The NTF classification method applied in LIBS achieved higher accuracy than the conventional SVM classification method, and the use of handheld LIBS better met the measurement requirements for certain narrow spaces.	30
Chalcopyrite, bornite, azurite, beryllium copper ore, and pyrite	LIBS and DRS data fusion	Hierarchical data fusion (MLDF) of LIBS and DRS data significantly improved the predictive capability of the model (with predictive indicators such as R^2 and REP all enhanced), fully demonstrating the enhancement effect of data fusion on LIBS predictive performance.	31
Minerals (pyrite, chalcocite, azurite, molybdenum ore, etc.)	PLSR, ANNR, and MCR-ALS	The nonlinear characteristics of ANN were utilized to optimize mineral classification, and ANNR exhibited the best model prediction performance, improving the prediction accuracy of conventional LIBS instruments.	32
Minerals (dolomite, zoisite, chalcopyrite, pyrrhotite, platinum-palladium copper ore, etc.)	PCA	Distribution maps generated by combining LIBS with PCA were compared with SEM-EDS pre-imaging, showing good consistency. This verified the effectiveness of the LIBS instrument in real-time monitoring and automated mineral phase identification.	33
Quartz, granite, shale, limonite, and hematite	PCA and BP-ANN	Combining LIBS with either PCA or BP-ANN achieved 100% prediction accuracy for five types of ores, fully demonstrating the nonlinear predictive capability of BP-ANN.	34
Iron ore (containing TFe, SiO_2, Al_2O_3, and P)	Cassegrain telescope (for LIBS optical system), OWS algorithm	The spectral preprocessing algorithm was optimized using the Overlapping Window Sliding (OWS) algorithm, and two normalization steps were implemented to improve the stability of spectral data.	35
Iron ore slurry	MsWT-LCNN	After adopting the MsWT-LCNN prediction method, the MAE of the validation set was only 0.93%, which significantly improved the accuracy of LIBS-based on-site online mineral analysis.	36
Mars analogs (basalt, andesite, etc.)	CF-LIBS	CF-LIBS detection was performed on Martian analog rock samples, demonstrating the potential of the equipment for qualitative and quantitative analysis of silicate ores in thin terrestrial atmospheres.	37
Volcanic ash	CF-LIBS	CF-LIBS technology was used for compositional detection of volcanic ash from multiple locations. Calculations based on the LTE assumption reduced self-absorption effects, verifying the feasibility of this technology for real-time detection in volcanic environments and thus contributing to active volcano monitoring.	38,39

Coal production process monitoring. The production of coal remains a crucial component of industrial operations. This is primarily because coal, as one of the world's major energy sources, plays a vital role in electricity generation; and in many countries,

electricity supply continues to depend heavily on coal-fired power plants. Given coal's importance in industrial production, key parameters such as unburned carbon (UC) content, calorific value of coal (Qad), and ash (Aad) content must be continuously monitored, with control parameters automatically adjusted to enhance production efficiency and quality, thereby ensuring smooth and stable operations[9]. Consequently, real-time monitoring of the coal production process has become a prominent research focus in recent years, and LIBS, due to its significant advantages in real-time monitoring, has been progressively adopted in major coal production processes.

As early as 2001, Body *et al.*[40] developed a variant of the LIBS system equipped with multiple CCD modules capable of simultaneously determining multiple elements. This system demonstrated rapid coal composition analysis and incorporated several data preprocessing techniques—such as pulse-to-pulse intensity normalization and data filtering—to minimize experimental error. Their experiments confirmed that pulse-to-pulse intensity normalization enhanced ease of operation and clearly demonstrated the potential of LIBS for real-time coal monitoring. One year later, Chadwick *et al.*[41] applied a LIBS analyzer to commercial coal analysis, conducting one month of independent testing. Their study showed a strong correlation between LIBS results for ash-forming elements extracted from coal using acid extraction and demonstrated good stability throughout the testing period. In the same year, Noda M.'s team[42] developed a fully automated LIBS system for monitoring carbon content in fly ash, coke, and pulverized coal in power plants. Compared with conventional Japanese methods (JIS-8814 and JIS-8815), their LIBS device achieved equivalent results within one minute, reducing the analysis time from 30 minutes, and thus exhibited exceptional detection efficiency.

In 2003, Kurihara *et al.*[43] developed a device for real-time monitoring of UC content in coal, as illustrated in Fig. 4. The system consists of a measuring head housing a laser and a control box containing a measurement control unit. By analyzing signal strength, the device determines the concentrations of carbon, silicon, calcium, aluminum, and iron in fly ash and calculates UC content from these concentrations, using it as a feedback factor to optimize and stabilize boiler combustion control. The team also deployed this LIBS device in a 1000 MW power plant, where experimental results demonstrated consistency between LIBS measurements and those obtained using conventional standard methods, thereby validating LIBS's effectiveness and feasibility for real-time coal parameter monitoring in power plants.

Although LIBS, as an emerging online analytical device at the time, exhibited clear advantages in real-time performance, portability, and accuracy, mainstream elemental analysis techniques then remained prompt gamma neutron activation analysis (PGNAA) and X-ray fluorescence spectrometry (XRF).

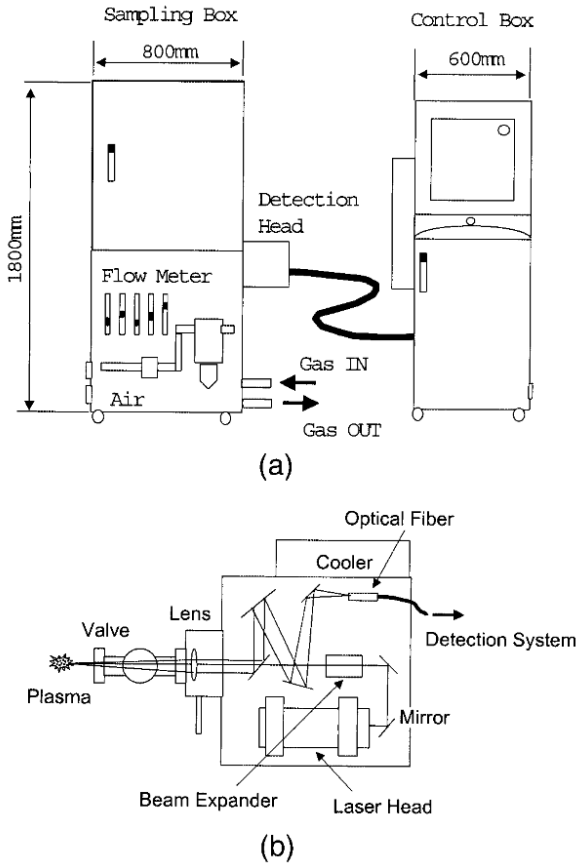

Fig. 4 Unburned carbon measuring instruments: (a) system configuration, (b) optical unit (adapted from [43]).

As the unique benefits of LIBS became more widely recognized through comparisons with these conventional techniques, LIBS gradually gained acceptance.

In 2008, Gaft *et al.*[20] developed a LIBS monitoring system and compared it against PGNAA. Laboratory data from both techniques served as a benchmark in a four-month field trial at Optimum Colliery in South Africa. The results demonstrated that LIBS achieved accuracy and error levels comparable to PGNAA for online ash content analysis of coal on a moving belt conveyor, and both systems yielded an average standard error of 0.32%, consistent with industrial requirements. Furthermore, LIBS offered higher safety and lighter weight compared with PGNAA.

Two years later, Gurjar [44] confirmed the feasibility of LIBS for real-time coal quality monitoring across multiple aspects, including safety, sample preprocessing, and error optimization, highlighting its potential to replace PGNAA and XRF. He developed a calibration approach for coal samples, successfully generating linear calibration curves for elements such as C, Si, and Al, and verified LIBS's capability to accurately quantify these elements. He also demonstrated LIBS's ability to analyze trace

elements such as Na and K, which is critical for industrial online coal elemental analysis. Subsequently, Romero *et al.*[45] integrated LIBS with a temperature prediction neural network for monitoring coal quality both in laboratories and power plants. Their results showed that, in coal-fired plants, the average prediction accuracy for temperature using LIBS was $\pm 14\ ^{\circ}C$, with a prediction error of $\pm 56\ ^{\circ}C$.

In 2012, Zhang. *et al.*[9] reviewed progress in LIBS-based online monitoring of UC in pulverized coal and fly ash and presented a LIBS system for real-time coal quality monitoring in power plants. This system measured elements including C, Ca, Mg, Ti, Si, H, Al, Fe, and oxygen in organic matter and developed mathematical models to convert elemental compositions into approximate analytical forms for calculating coal calorific value (Q_{ad}) and ash content (A_{ad}). They also proposed a formula for estimating C-line intensity (I_c) to mitigate spectral interferences and matrix effects, thereby improving UC analysis accuracy. Their results reported a correlation coefficient of 0.997 and a measurement error of 3.81%.

In 2015, Zhang *et al.*[46] introduced a closed-loop feedback system for stabilizing pulsed laser energy and conducted a one-month monitoring test. By maintaining Nd:YAG laser output energy within a preset range based on detected energy signals, they significantly improved LIBS's long-term stability for coal quality measurements. Around the same time, Redoglio *et al.*[47] tested a reflector-based, large-depth-of-field LIBS system for analyzing coal on moving belts under laboratory conditions simulating power plant environments. The system accurately quantified elemental content and improved flexibility in real-time monitoring. Similarly, Legnaioli S.'s team[48] evaluated LIBS for online ash analysis under simulated power plant conditions, combining it with an artificial neural network (ANN). Their approach achieved ash measurement accuracy better than $\pm 4\ wt\%$, meeting industrial standards.

In 2020, Ma *et al.*[49] applied double-pulse LIBS (DP-LIBS) in a helium environment for quantitative sulfur analysis in coal. This approach successfully enhanced sulfur spectral intensity, yielding results of $R^2 = 0.992$, LOD = 0.038 wt.%, and RMSECV = 0.143 wt.%. These evaluations under simulated industrial conditions highlighted LIBS's applicability to real-world coal-fired power plants. In 2021, Zhan K.'s team[50] developed a physically constrained sample preparation device for coal dust, ensuring consistent surface flatness and stability during ablation. This device reduced sample preparation time to 30 seconds while improving analytical accuracy and efficiency in online coal analysis.

In recent years, researchers have increasingly combined LIBS with modeling approaches to enhance measurement precision. For example, Ni *et al.*[51] compared four calibration models—support vector regression (SVR), back-propagation neural networks (BP), random forests (RF), and partial least squares regression (PLSR). Their findings indicated that SVR and BP produced the most accurate results, while PLSR offered faster training speed and stable predictions. Dou *et al.*[52] assessed three dataset partitioning strategies—random selection (RS), Kennard–Stone (KS), and sample partitioning based on X–Y joint distance (SPXY)—in combination with PLSR, SVR, and RF. They concluded that SPXY coupled with RF yielded superior performance. Liu R.'s team[53] applied transfer learning to PLS modeling for real-time monitoring of moisture (M_{ad}), ash (A_d), sulfur (S_t), and calorific value (Q) in coal briquettes across four production lines. Their study demonstrated that increasing sampling frequency improved efficiency without compromising accuracy, significantly reducing operational costs. Additionally, Tian *et al.*[54] integrated XRF with LIBS to enable effective analysis of organic elements such as C and H in coal while improving the stability of inorganic ash-forming element detection.

Despite these advantages, challenges remain for online coal analysis in real industrial environments. As noted by Zhang *et al.*[9], coal's heterogeneity and irregular particle shapes cause substantial spectral signal variability, while interference from the O I 926.1 nm line limits sulfur detection, resulting in insufficient detection sensitivity for sulfur quantification. Continued research has partially addressed these issues: for example, the large-depth-of-field system developed by Redoglio D.'s team[47] effectively mitigates stability problems caused by plasma–detector angular changes due to coal heterogeneity, while Ma Y.'s DP-LIBS system[49] enhances sulfur spectral intensity and improves detection sensitivity. Nonetheless, DP-LIBS remains limited in practical deployment, and many facilities lack suitable conditions for large-depth-of-field systems. Further development of instrumentation and methodologies is therefore required to improve reproducibility and stability.

In summary, the application of LIBS technology in the coal industry has evolved from fundamental compositional analysis to the current sophisticated stages of closed-loop control and multi-model fusion. To provide a structured comparison of the aforementioned literature regarding LIBS-based online coal monitoring, Table 2 categorizes these studies across two dimensions: the core methodologies employed (encompassing both hardware optimization and algorithmic models) and their primary research contributions.

Steel production process monitoring. As the cornerstone of modern industrial society, steel is extensively utilized across diverse sectors—including construction, manufacturing, infrastructure development, and national defense—rendering its strategic importance indisputable. During the steel production process, precise real-time elemental monitoring not only facilitates enhanced production efficiency and optimized raw material proportions but also significantly reduces operational costs while

Table. 2 The contributions of various studies in the field of LIBS for real-time monitoring of coal materials

Methods	Contributions	Refs
Multi-CCD module LIBS with pulse-to-pulse intensity normalization and data filtering preprocessing.	Demonstrated the capability for rapid coal composition analysis and the potential of LIBS equipment for real-time monitoring.	40
Design of a commercial-grade LIBS analyzer.	Conducted one month of independent testing, demonstrating excellent operational stability.	41
Development of an automated LIBS analytical system.	Showcased higher efficiency for online detection compared to traditional techniques (e.g., JIS-M8814) and the ability to detect carbon under high-pressure, harsh conditions.	42
Real-time LIBS monitoring device for Unburned Carbon (UC).	Utilized real-time UC data as a feedback factor for stabilizing boiler combustion to achieve quality control; field deployment at a power plant proved effectiveness.	43
Online in-situ LIBS analysis.	Following 4 months of field measurements and comparison with PGNAA results, the precision and error levels were found to be comparable to traditional techniques.	20
PCA analysis of data generated by LIBS monitoring equipment.	Confirmed the feasibility of replacing PGNAA and XRF for coal quality monitoring; detailed linear ranges for various elements and identified trace elements (e.g., Na, K); recommended nano-powder for calibration and provided procedures to address signal nonlinearity.	44
Online LIBS monitoring equipment integrated with Temperature Neural Networks.	Field-tested an online analysis system, proving the feasibility of coal ash composition measurement and the possibility of predicting coal slagging using the integrated model.	45
Automated LIBS analytical prototype.	Reviewed progress in online equipment for pulverized coal and fly ash UC; developed a prototype using second-order polynomial multivariate inverse regression to mitigate matrix effects.	9,46
Large Depth-of-Field (DOF) LIBS system based on reflective mirrors.	Simulated coal-fired power plant environments in the laboratory to test the equipment; the mirror-based design significantly improved system flexibility.	47
LIBS coupled with Artificial Neural Networks (ANN).	Laboratory simulation of industrial power plant conditions; demonstrated excellent consistency between predicted and standard values after ANN processing.	48
Double-pulse LIBS (DP-LIBS).	Successfully enhanced sulfur spectral line intensity via DP-LIBS in a helium environment (R^2=0.992, LOD=0.038 wt.%, RMSECV=0.143 wt.%).	49
Physical constraint preparation of coal powder with PLSR model for LIBS data prediction.	Improved detection repeatability through physical constraints; the best average Relative Standard Deviation (RSD) was <5%.	50
Four chemometric methods for carbon content calibration (SVR, RF, BP, PLSR).	RF performed worst; SVR and BP were identified as the most promising calibration models, while PLSR offered better stability and faster training (SVR: R^2=0.95, RMSEP=0.17; BP: R^2=0.95, RMSEP=0.16; PLSR: R^2=0.92, RMSEP=0.19).	51
Three dataset partitioning methods (RS, KS, SPXY) and three predictive models (PLSR, SVR, RF).	The combination of Sample Set Partitioning based on Joint X-Y Distance (SPXY) and Random Forest (RF) yielded superior results (Aad: R^2=0.984; Q: R^2=0.984; Volatiles: R^2=0.980).	52
Transfer Learning combined with Partial Least Squares (PLS) for LIBS.	Performed transfer learning calibration across 4 identical online LIBS systems; maintained high precision without sample preparation (Mad: MAE<0.55 wt.%; Aad: MAE<1.50 wt.%; St: MAE<0.10 wt.%; Q: MAE<1 MJ/kg).	53
Hybrid XRF-LIBS system.	Combined LIBS for direct analysis of organic elements (C, H) with XRF to compensate for LIBS instability in detecting inorganic ash-forming elements, achieving high repeatability (C: R^2=0.99, RSD=0.15%; Q: R^2=0.97, RSD=0.11 MJ/kg).	54

ensuring product quality. Consequently, the implementation of real-time monitoring for various elements in steel production has become increasingly critical, providing essential support for the rigorous control and continuous optimization of the manufacturing process[55].

Between 2001 and 2004, Gruber *et al.*[56–58] introduced a LIBS system capable of rapid in situ analysis of both solid and molten metals from a distance of 1.5 meters. This device enabled real-time monitoring of Cr, Cu, Mn, and Ni in liquid steel. It is important to note, however, that this approach analyzes only the liquid surface, which can introduce measurement errors. Moreover, oversaturated I/I_{ref} values may lead to issues such as self-absorption effects, which must be addressed. LIBS equipment was utilized to perform rapid on-site analysis of both solid and molten metal in vacuum degassing (VD) and vacuum induction melting (VIM) processes within low-pressure plant environments. The results indicated that LIBS measurements on the VD system exhibited a strong

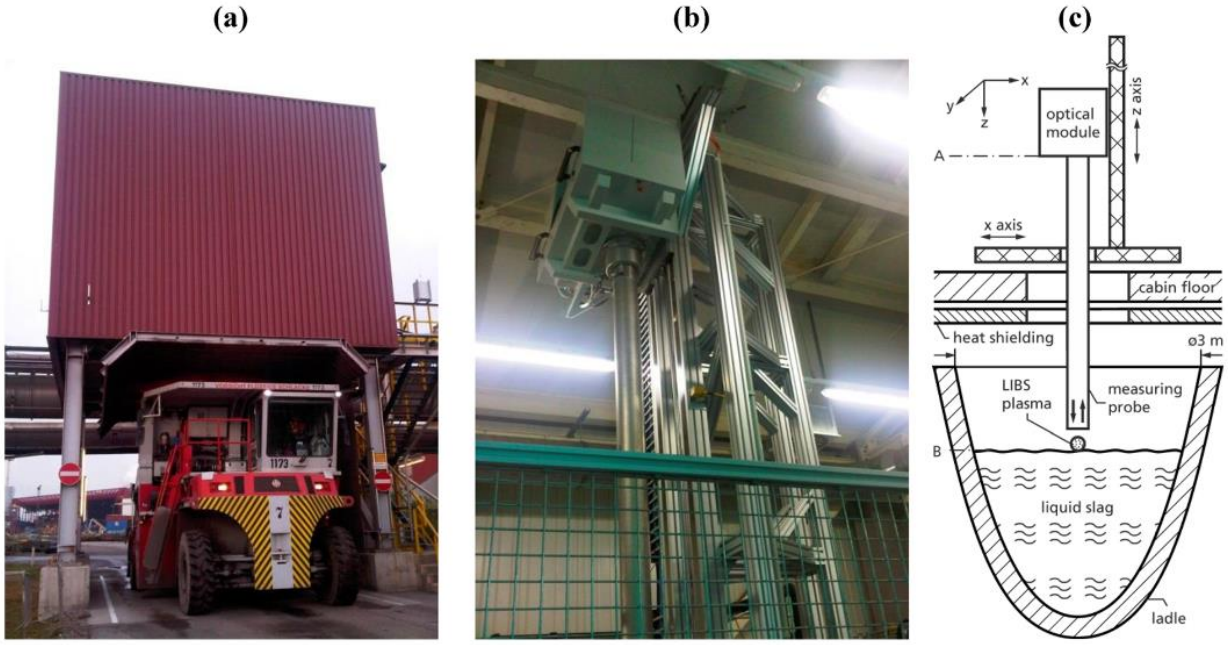

Fig. 5 Unburned carbon measuring instruments: (a) system configuration, (b) optical unit (adapted from [43]).

correlation exclusively for Ni. The low-pressure conditions substantially reduced analytical accuracy, limiting data volume and preventing the establishment of calibration curves. Nonetheless, variations in the concentration of specific elements could be tracked following alloying additions.

In 2006, Hubmer *et al.*[19] developed a process optimization and control system known as VAI-CON Chem, integrating it with a LIBS analytical platform for quasi-continuous chemical analysis of liquid high-alloy steels. The system achieved relative average residuals (R_{rel}) for Cr, Ni, and Mo below 0.038 and absolute average residuals (R_{abs}) below 0.198, with errors for Cr and Ni lower than those in concurrent studies.

CHEN *et al.*[59] compared laser plasma spectra of industrial liquid steel under atmospheric and argon environments. They constructed calibration curves for Mn, Si, and Cr, with linear correlation coefficients exceeding 0.925, and detection limits of 75.7 μg/g, 23.8 μg/g, and 724.5 μg/g, respectively. Their findings demonstrated that an argon environment not only prevents oxidation of the steel surface but also enhances spectral line intensities, thereby improving the feasibility of direct and real-time composition measurements of liquid steel.

However, early studies at that time could only preliminarily demonstrate the feasibility of LIBS instruments for monitoring steel processing. Subsequently, the research focuses gradually shifted toward enhancing the operational efficiency of industrial steel manufacturing processes and improving the monitoring stability of LIBS systems.

In 2013, Sun *et al.*[60] developed a LIBS-based online prototype for liquid steel analysis and established calibration curves for Cr, Ni, Si, and Mn. They observed that when molten steel temperatures exceeded 1200 °C, most spectral line intensities increased significantly, and the detection sensitivity for minor elements in liquid steel surpassed that of solid steel. However, spectral lines in liquid steel were more prone to saturation, resulting in narrower linear ranges for the calibration curves. In their 2015 study[61], the team integrated a Cassegrain telescope with double-pulse laser operation to develop an in situ LIBS analysis system, using a univariate PLS calibration model for elemental quantification in liquid steel. The PLS model produced root mean square errors of prediction (RMSEP) of approximately 5% and average relative standard deviations (RSDs) of 2–3%. When tested in steel mills, the LIBS system achieved high accuracy for C, Si, and Mn measurements, with errors below 0.02%, meeting industrial standards.

Sturm *et al.*[62] applied LIBS to monitor liquid steel slag in harsh environments between 600–1400 °C, performing online analysis of slag elements including CaO, Fe, and SiO_2. Fig. 5 illustrates the slag transport steps and LIBS instrumentation for slag monitoring. Measurement involved device fixation, activation, automatic probe release, and optical module positioning at the slag surface. The study revealed that, even at significantly increased measurement distances, RMSEP values for liquid slag remained comparable to other experiments, and the maximum RMSEP was only twice that of solid slag measurements.

In 2015, Lorenzetti *et al.*[63] combined LIBS with artificial neural

network (ANN) algorithms for continuous monitoring of transition castings in continuous casting machines. Their findings demonstrated that coupling LIBS with ANN significantly improved the time efficiency of spectral analysis, thereby accelerating production processes. Similarly, in 2017, Ruiz *et al.*[64] employed a double-pulse LIBS system for real-time monitoring of compositional transitions during continuous casting in steel mills. Using discriminant function analysis (DFA) to interpret spectra, the study successfully identified steel grades with small compositional differences and detected changes in steel composition as low as 0.20%.

Subsequently, Cabalín *et al.*[65] implemented a portable discrete LIBS system at a steel plant in Spain, also combined with DFA to distinguish steel grades during continuous casting. Their experiments showed that a single laser pulse effectively removed oxide layers and casting powder residues, exposing the steel matrix and producing satisfactory analytical results. However, limitations included interference from elements within the oxide and abrasive powders (*e.g.*, Mn, Ti, Si), and difficulty distinguishing the first three steel grade groups when Cr content was below 1.3%, restricting accurate identification to the latter three grades.

Wang *et al.*[66] investigated remote open-path LIBS under varying temperatures, lens-to-sample distances (LTD), and sample angles, and characterized its online measurement performance. They proposed a three-dimensional profiling system based on parallel laser beam streak projection to assess sample profiles at different temperatures.

More recently, an Iranian team[67] combined numerical simulations of the Goldak model with real-time LIBS monitoring to analyze molten steel pool dynamics. This approach provided precise data on localized molten pool temperature and elemental composition. Their results indicated that monitoring spectral intensity ratios enabled real-time control of input parameters, ensuring the production of high-quality cladding layers with targeted dilution levels for industrial applications. Sdvizhenskii P. A.'s team[68] subsequently applied LIBS to hot pig iron analysis to examine the influence of melt temperature on analytical performance. Their experiments revealed that increasing melt temperature (1550 °C vs. 1350 °C) enhanced spectral intensity, improved calibration curve linearity, and reduced analytical errors. This improvement was attributed to better mixing and homogenization of the melt at elevated temperatures, without significant changes in plasma temperature.

In conclusion, the application of LIBS technology in steel production has expanded to encompass full-process monitoring, ranging from the elemental analysis of molten steel and slag to the grade identification of continuous casting products. By incorporating advanced methodologies—such as the introduction of double-pulse techniques, the implementation of novel optical systems[61], and the utilization of auxiliary algorithms[63,64]—researchers have consistently overcome interferences arising from high temperatures, surface oxidation layers, and complex matrix effects. Table 3 provides a systematic summary of the methodologies and research contributions presented in the aforementioned representative literature.

Other Alloy Smelting Process Monitoring. In addition to the real-time monitoring of elemental composition during the smelting of alloys such as iron and steel, numerous studies have also investigated the application of LIBS for online monitoring of other alloys, including magnesium and aluminum alloys. These alloys are widely used in aerospace, automotive, electronics, and defense industries[69,70], and consequently, close attention has been directed toward operational control in their production processes.

In 2005, supported by ERCo Energy Research, Saro *et al.*[71,72] evaluated the capability of LIBS probes to measure the composition of aluminum, steel, and glass melts within industrial furnaces. Their findings indicated that LIBS exhibited accuracy comparable to that of traditional spark spectrometers and XRF techniques. In addition, the study addressed the underlying principles of LIBS, its cost, operational challenges, measurement precision, and energy savings potential. The results showed that analytical errors for materials such as aluminum and glass were within industry-accepted limits. The study also projected that, by 2010, the adoption of LIBS devices could save approximately 1.44 trillion Btu annually in the aluminum industry and 17–45 trillion Btu per year in the glass industry compared with conventional systems.

Similarly, research at that time only proved the feasibility of LIBS for processing materials such as alloys. However, alloy manufacturing is typically accompanied by harsh conditions, including high temperatures and pressures. To evaluate the adaptability of LIBS instruments within such environments, Zeng *et al.*[73] focused on online LIBS monitoring of molten aluminum and other metals to detect solid corrosion within equipment under high-temperature conditions. Their study successfully monitored changes in the composition of molten aluminum within a stainless steel crucible at temperatures up to 1000 °C, thereby confirming LIBS as an effective tool for investigating the corrosion mechanisms of solid materials in molten metal environments. Furthermore, Gudmundsson *et al.*[74,75] monitored 14 trace elements in a primary aluminum smelter and achieved concentration accuracies ranging from 2 to 8 ppm in terms of relative concentration. Their results demonstrated that LIBS can reliably quantify high-vapor-pressure elements, such as Na and Mg, at the ppm level. A comparison with conventional optical emission spectrometry (OES) further revealed that LIBS measurements were comparable to offline laboratory OES analysis in terms of both accuracy and precision.

Table 3. The contributions of various studies in the field of LIBS for real-time monitoring of steel production process

Methods	Contributions	Refs
Rapid in-situ LIBS analysis at a distance of 1.5 meters.	Conducted rapid in-situ LIBS analysis of liquid and solid steel under atmospheric and low-pressure industrial environments. Although some errors occurred during liquid steel analysis, the results demonstrated the potential of LIBS for rapid in-situ analysis in industrial settings. Results under standard pressure are as follows: Cr: LOD = 0.053 wt.% Cu: LOD = 0.054 wt.% Mn: LOD = 0.104 wt.% Ni: LOD = 0.207 wt.%	56–58
Process optimization control system named "VAI-CON Chem".	Reduced errors in the online analysis of multiple elements (Cr, Ni, Mo, Cu, Co) by integrating the developed control system with the LIBS apparatus. Performance metrics: R_{rel}<0.038, R_{abs}<0.198.	19
Online monitoring under an argon atmosphere.	Demonstrated that an argon environment not only prevents the oxidation of molten steel but also enhances spectral intensity. Mn: R^2=0.987, LOD = 75.7 μg/g Si: R^2=0.956, LOD = 23.8 μg/g Cr: R^2=0.927, LOD = 724.5 μg/g	59
Development of a prototype LIBS device for online liquid steel analysis.	Temperature significantly affects spectral intensity, with varying impacts across different elements. Increasing sample temperature can improve the detection limits for certain elements; however, the linear range for some elements narrows at high temperatures. Cr: R^2=0.9998, LOD = 159 ppm, RSD = 4.98% Ni: R^2=0.9999, LOD = 70 ppm, RSD = 10.64% Si: R^2=0.9963, LOD = 41 ppm, RSD = 7.88% Mn: R^2=1.0000, LOD = 245 ppm, RSD = 7.26%	60
Cassegrain telescope integrated with double-pulse LIBS (DP-LIBS) combined with univariate and PLS models.	The online DP-LIBS analyzer, equipped with a refractory lance, allows the opto-electrical system to be positioned away from high-heat zones, significantly reducing maintenance costs. Double-pulse excitation not only enhances signal intensity but also reduces intensity fluctuations. The PLS model outperformed the univariate model in terms of accuracy and repeatability. The RSD for Si, Mn, Cr, Ni, and V elements ranged between 2%-3%, with an RMSEP of approximately 5%.	61
Online analysis of molten steel slag using LIBS in harsh environments (600–1400 °C).	Three-month online trial results showed an RSD of 1.7%-2.2%, exhibiting excellent measurement repeatability. Despite a significant increase in measurement distance, the RMSEP for solid slag remained low, confirming the high flexibility and environmental adaptability of LIBS equipment.	62
ANN integrated with LIBS.	Combining LIBS with Artificial Neural Network (ANN) algorithms significantly improved spectral analysis efficiency, facilitating the acceleration of the overall production process.	63
DP-LIBS combined with DFA for steel grade identification in continuous casting.	Discriminant Function Analysis (DFA) of LIBS spectra enabled accurate identification of steel grades with minor elemental variations. It can detect compositional changes as low as 0.2%, helping to reduce the production of downgraded steel and lower plant energy consumption and costs.	64
DFA for steel grade identification in continuous casting.	A single laser pulse was used to remove the thick oxide layer on the molten steel surface to access the steel matrix, thereby reducing measurement errors. The field results showed high consistency with laboratory results obtained using laser interferometry.	65
Proposed a 3D profile measurement system using parallel laser beam fringe projection and an innovative coaxial laser beam system.	Emission intensity decreased when the lens-to-target distance or sample angle deviated from design values, proving the robustness of the remote open-path LIBS system. Additionally, the feasibility of the 3D profile measurement system was validated.	66
Numerical simulation based on the Goldak model combined with LIBS.	Plasma temperature extracted from Cr emission lines effectively tracked changes in melt pool temperature (an input parameter). The Ni/Fe intensity ratio quantified the dilution level of the cladding layer, ensuring consistent cladding quality within the melt pool.	67
LIBS monitoring of hot pig iron.	For the Si content calibration curve in pig iron, higher melt surface temperatures led to improved precision and linearity. At elevated surface temperatures, the emissivity of the laser-induced plasma spectrum was higher—a phenomenon that cannot be explained solely by plasma temperature or electron density.	68

Xin *et al.*[76] designed a double-pulse LIBS system to monitor the composition of magnesium alloys during smelting for the first time. The relative standard deviations for yttrium (Y), praseodymium (Pr), and zirconium (Zr) were all below 10%. Although the calibration performance for molten magnesium alloys was inferior to that for solid samples, the study nevertheless provided valuable insights for future online monitoring of molten magnesium alloys in industrial settings.

The aforementioned studies provide empirical evidence confirming the feasibility and robustness of LIBS for real-time monitoring during alloy processing. Consequently, LIBS technology has undergone rapid expansion toward the detection of a broader range of alloy categories in this field. For instance, Baril *et al.*[77] developed a LIBS-based method for continuous in situ analysis of galvanizing baths and partially molten metals, demonstrating the feasibility of LIBS for bath management and the monitoring of dissolved chemicals. Myakalwar *et al.*[78]

successfully employed high-energy laser pulses in LIBS to monitor the desulfurization of vesiculated copper in the molten state. The results accurately determined the critical desulfurization endpoint, offering key information for process control. Their findings also indicated that LIBS offered advantages over differential optical absorption spectroscopy (DOAS) in terms of simplicity and reduced measurement delay.

In late 2024, Liu's team[79] integrated programmable logic controllers (PLCs) with a machine-learning-assisted LIBS system for online monitoring of multiple elements in hot-dip galvanizing solutions. By applying normalization and Principal Component Analysis–Mahalanobis Distance (PCA-MD) filtering to remove anomalous spectra, the accuracy of the measurements was markedly improved. Furthermore, Random Forest predictive models for aluminum, magnesium, and iron in hot-dip galvanizing solutions achieved R^2 values exceeding 0.9932 and root mean square errors below 0.0013%, thereby demonstrating the strong potential of machine-learning-assisted LIBS for online analysis in such solutions.

In the same year, Spencer *et al.*[80] conducted LIBS measurements of compositional gradients in aluminum-copper sputtered alloys using a pulsed femtosecond laser and a gated sCMOS detector for alloy grading. Energy-dispersive spectroscopy (EDS) was employed to validate the calibration of the LIBS results, with an average percentage error of only 1.4% between LIBS and EDS data. One year later, Liu J.'s team[81] applied femtosecond LIBS to the quantitative analysis of magnesium alloys and simultaneously evaluated the performance of four classification models: Random Forest (RF), Support Vector Machines (SVMs), Partial Least Squares (PLS), and k-Nearest Neighbors (KNN). Their findings showed that the Random Forest Regression (RFR) model exhibited strong predictive accuracy, achieving R^2 values ≥ 0.74, RMSE below 8.269, and MRE below 18.200, while the Random Forest Classification (RFC) model demonstrated superior performance on imbalanced datasets.

These two studies underscore the application of femtosecond LIBS in alloy detection. While femtosecond LIBS provides high repetition rates and rapid detection speed, its sensitivity can be limited. To address this, Liu's team[81] implemented femtosecond laser ablation–spark-induced breakdown spectroscopy (fs-LA-SIBS), which employs spark discharges to enhance plasma radiation. This approach significantly improved sensitivity while maintaining the high-speed advantage of femtosecond LIBS, thereby better meeting the demands of rapid in situ monitoring. Table 4 provides a comprehensive summary of the contributions of the literature discussed in this section to real-time LIBS monitoring, categorized by alloy type and analytical methodology.

Real-Time Industrial Waste Monitoring. As global industrialization accelerates, it has driven advancements in science and technology, economic growth, and enhanced competitiveness. However, it has simultaneously given rise to pressing challenges, including water pollution, excessive resource consumption, and climate change, as well as social issues such as class division and urbanization. While industrialization has generated substantial economic benefits for society, the accompanying environmental and social problems cannot be overlooked[82–84]. Addressing these issues has become a major focus in recent years, and the development of effective methods for real-time monitoring of pollution sources arising from hazardous wastewater and waste disposal in industrial production has facilitated notable progress in this field.

As early as 1997, Singh *et al.*[85] applied LIBS to real-time monitoring of exhaust gas streams at a thermal treatment test facility. By tracking the concentration of specific toxic metals in exhaust gases, they demonstrated the feasibility of LIBS as a remote monitoring tool for waste treatment process control.

To enhance the detection precision of LIBS instruments, in the same year, Hahn *et al.*[86] developed a prototype in-situ metal monitor based on LIBS optics for detecting metal emissions in wastewater. Field testing of this monitor at a pyrolysis wastewater treatment facility in California revealed robust performance in waste treatment monitoring. Subsequently, the same team proposed a random sampling and conditional analysis approach for wastewater monitoring, supported by Monte Carlo simulations, which improved the sensitivity and applicability of LIBS wastewater analysis by approximately an order of magnitude[87]. Although LIBS remains less sensitive than mature techniques such as ICP/AES, its low sample destructiveness and in-situ capabilities render it highly suitable for real-time monitoring applications.

Zhang *et al.*[88] tested LIBS on an EPA incinerator for exhaust gas monitoring, validating its effectiveness for real-time monitoring, though accuracy still required improvement. Kumar *et al.*[89] utilized a MATLAB-based CF-LIBS algorithm to monitor industrial wastewater, and their results were consistent with those obtained using traditional calibration-curve methods, thereby enhancing the flexibility of LIBS in online analysis. Similarly, Dutouquet C.'s team[90] demonstrated LIBS's potential for directly measuring copper emissions in real time. Despite observable matrix effects, the consistency of calibration curves indicated that the impact was limited, achieving detection limits of 15 $\mu g/m^3$ and 20 $\mu g/m^3$ in both laboratory and field analyses.

Between 2021 and 2022, Garcia's team[91] and Tognana's team[92] applied LIBS to copper detection in electronic waste and plastic waste, respectively. Garcia's team showed that LIBS could serve as an alternative to the copper leaching process for electronic equipment waste, offering a simpler procedure than ICP-MS and eliminating the need for additional reagents. Meanwhile, Tognana's team successfully detected copper in plastic waste

Table 4. The contributions of various studies in the field of LIBS for real-time monitoring of other alloy smelting process

Primary Alloy Components	Contributions	Refs
Aluminum, steel, and glass melts	LIBS was employed to measure alloy components in industrial furnaces. Comparison with traditional spark-OES and XRF results showed comparable precision. It was reported that the new LIBS-based equipment could significantly reduce energy consumption in the aluminum, glass, and steel industries.	[71,72]
Molten aluminum	LIBS enables online diagnosis of corrosion behavior in molten metals by monitoring changes in characteristic spectral line intensities. This confirms LIBS as an effective technique for studying the corrosion mechanisms of solid materials in molten metal environments.	[73]
Molten aluminum and other alloys	Monitored the concentration of 14 trace elements in smelters with ppm-level precision. The results demonstrated the reliability of LIBS for measuring relative concentrations of elements with high vapor pressure (*e.g.*, Na, K). The accuracy and precision of LIBS measurements were found to be comparable to offline laboratory OES analysis.	[74,75]
Molten magnesium alloys	Developed a stand-off LIBS system capable of long-distance focusing, collection, and imaging. This marked the first-ever monitoring of magnesium alloy components during the smelting process. Results at a detection distance of 1.89 m were as follows: Pr: R^2=0.990, RSD=6.26%, LOD=937 ppm Zr: R^2=0.995, RSD=9.84%, LOD=334 ppm Y: R^2=0.986, RSD=6.85%, LOD=864 ppm	[76]
Dissolved aluminum and galvanizing baths	Validated the feasibility of the developed LIBS apparatus for water bath management and monitoring of dissolved chemicals.	[77]
Blister copper	Confirmed that stand-off LIBS (ST-LIBS) is suitable for real-time monitoring of the desulfurization process in molten blister copper. Real-time monitoring of sulfur at ppm levels was achieved for the first time. The results were validated using Differential Optical Absorption Spectroscopy (DOAS), with LIBS showing superior advantages in terms of simplicity and measurement latency.	[78]
Hot-dip galvanizing solution	Developed a machine learning-assisted LIBS system integrated with a Programmable Logic Controller (PLC). The PCA-MD method was utilized to enhance data accuracy. The RF prediction models for Al, Mg, and Fe yielded R2 values exceeding 0.9932, with RMSECV consistently below 0.0013%.	[79]
Al-Cu sputtered alloys	Performed LIBS measurements on Al-Cu sputtered alloys using a pulsed femtosecond laser and a gated sCMOS detector. The results were validated using Energy Dispersive Spectroscopy (EDS), showing an average percentage error of only 1.4%.	[80]
Magnesium alloys	Conducted LIBS analysis using femtosecond laser ablation spark-induced breakdown spectroscopy. Data analysis was performed using four chemometric methods (RF, SVM, and KNN), with the Random Forest Classifier (RFC) model yielding the optimal classification performance.	[81]

without additional reagents, highlighting LIBS's potential for monitoring copper in such waste streams.

Given its capabilities for rapid in-situ analysis and high environmental adaptability, LIBS has also seen significant development in nuclear off-gas emission monitoring and other related fields. Andrews's team[93] applied LIBS to monitor aerosolized Xe, Kr, Cs, and Rb particles in the waste streams of molten salt reactors (MSRs). Univariate peak models for Xe and Kr exhibited strong correlations with elemental concentrations. In addition, multivariate models for all four analytes were developed using Partial Least Squares (PLS) regression combined with preprocessing steps, yielding prediction confidence intervals of 99.9%. A real-time test involving adjustments to Kr mass flow rates produced root mean square errors of prediction (RMSEP) of 0.051 mol%, 0.060 mol%, and 0.121 mol%, respectively. In another study, the team evaluated the effect of Ar and He atmospheres on trace Xe and Kr monitoring. They observed that plasma temperatures and electron densities were higher in Ar than in He, leading to extended plasma lifetimes, while prediction accuracy remained high in both atmospheres[94]. The team also investigated isotope quantification in MSR exhaust gases, developing a multivariate model for isotope ratios and subsequently refining it to reduce calibration sample requirements to just 18% of the original dataset[95]. Further experiments included real-time LIBS monitoring of hydrogen isotope shifts and elemental composition within molten salts. Using isotope-controlled experiments, they validated the relationship between diffusion rates and molecular weight, enabling quantitative estimation of D/H ratios in salts and offering deeper insights into the chemical processes within salt containers[96]. These studies collectively demonstrated LIBS's suitability for real-time MSR

waste gas monitoring and validated the predictive accuracy of associated transport models, offering valuable guidance for developing gas-phase LIBS monitoring frameworks.

In 2023, Elhassan *et al.*[97] investigated the application of LIBS for monitoring heavy metal removal from wastewater. They examined the effects of bentonite type, pollutant concentration, and adsorbent dosage on adsorption efficiency and confirmed the consistency between ICP-MS and LIBS results, reinforcing LIBS's capability for online real-time analysis of heavy metal wastes. In the same year, Bhatt *et al.*[98] collected wastewater samples daily from the foundation of a historic building over a 10-day period and analyzed them using a benchtop LIBS system equipped with a probe. By applying Principal Component Analysis (PCA) and Linear Discriminant Analysis (LDA), they successfully differentiated samples and quantified Fe content in the wastewater. Their results showed that the difference between LIBS and ICP-MS for Fe quantification was below 20%, underscoring LIBS's advantages in wastewater Fe analysis.

More recently, Chang's team[99] integrated LIBS with 3D scanning technology to analyze contaminants in Recovered Coarse Aggregate (RCA) derived from construction and demolition waste. This combined platform effectively addressed challenges posed by variations in laser emission angles and focal lengths caused by irregular object surfaces, thereby improving detection accuracy. Capela's team[100] applied LIBS to wood waste analysis, targeting contaminants such as arsenic, barium, cadmium, chromium, copper, mercury, lead, antimony, and titanium. Their experiments, which evaluated one to three spectral lines per element, revealed that the three-line standard method was the most reliable, particularly for elements with low detection sensitivity. Ultimately, they successfully identified three distinct types of contaminated wood waste.

In summary, LIBS technology has extensively permeated various critical stages of industrial waste management, spanning diverse scenarios such as incinerator off-gas monitoring, electronic and plastic waste recycling, and sophisticated effluent stream analysis in molten salt reactors. To provide a systematic overview, Table 5 categorizes representative research on LIBS-based real-time waste monitoring from recent years across three dimensions: the type of waste processed, the target monitored elements, and the primary research contributions.

This chapter provided a systematic review of the research progress of LIBS technology in fields such as mineral sorting and quantitative analysis, coal quality control, steel smelting, and industrial waste monitoring. Overall, by virtue of its distinct advantages—including minimal sample preparation, simultaneous multi-element detection, rapid in-situ response, and adaptability to harsh environments—LIBS has demonstrated immense potential and application value for the efficient monitoring and resource optimization of industrial production processes.

However, a series of challenges persist during its practical implementation. Specifically, the detection precision of LIBS remains limited for certain trace elements[38,39], and the technology still grapples with high measurement errors stemming from solid heterogeneity and non-uniform particle sizes[9]. Furthermore, the operational stability of LIBS instrumentation is hindered by interferences such as mold contamination and oxide layer formation during metallurgical processes. These issues, compounded by significantly low analytical accuracy caused by matrix effects and insufficient precision in liquid alloy detection[76], underscore the current limitations in the sensitivity and reliability of LIBS systems.

Consequently, future research in industrial production must focus on enhancing the accuracy and stability of LIBS equipment. Potential strategies include the application or development of superior algorithmic models for more precise predictions, the exploration of signal enhancement techniques (such as double-pulse LIBS), and the engineering of more robust, interference-resistant instrumentation to improve online analytical stability. Once these critical bottlenecks are optimized or resolved, LIBS is expected to find broader application in real-time monitoring sectors and experience even more rapid technological advancement.

ONLINE MONITORING OF LASER PROCESSING

Laser processing technologies, encompassing laser cleaning, materials processing, and welding, have flourished in recent years. Specifically, laser cleaning offers distinct advantages over traditional mechanical methods, including higher precision, superior efficiency, and an environmentally benign nature. Within this domain, laser paint removal has emerged as a critical technique in the aerospace and maritime industries[101,102], while laser materials processing continues to play a pivotal role in both traditional manufacturing and high-precision processing sectors. However, conventional offline inspection techniques frequently struggle to meet the stringent demands of modern industry for real-time monitoring of quality and efficiency during the laser manufacturing process. Given the rapid advancements in LIBS technology, the development of specialized equipment for the real-time monitoring and analysis of these processes has become indispensable. This section explores the evolutionary trajectory of LIBS instrumentation for real-time monitoring within the fields of laser cleaning and laser materials processing.

Real-time monitoring of laser cleaning. In 2000, Klein *et al.*[103]

Table. 5 The contributions of various studies in the field of LIBS for real-time monitoring of industrial waste

Waste Category	Target Elements	Contributions	Refs
Exhaust Gas	Cr, Pb, Fe, K, Mn, *etc.*	Demonstrated the capability of LIBS as a remote monitor in waste treatment by controlling plasma torches through the detection of specific toxic metal concentrations in exhaust gas.	85
Wastewater	Fe, Mn, Cr	Developed a LIBS-based in-situ metal monitor for wastewater discharge, showcasing robust performance in waste processing oversight.	86
Wastewater	Fe, Cd, Be	Proposed a stochastic sampling and conditional analysis method based on Monte Carlo simulations to significantly enhance sensitivity; concluded that the discreteness of metal particles in wastewater may limit real-time LIBS monitoring.	87
Exhaust Gas	Cr, Pb, Cd, Be	Confirmed the immediacy of LIBS as a real-time monitor through field tests on an EPA incinerator for exhaust gas analysis.	88
Wastewater	Cr, Pb, *etc.*	Utilized MATLAB-based data calibration for CF-LIBS (Calibration-Free LIBS), improving online analytical flexibility; results indicated that toxic elements like Cr and Pb exceeded regulatory limits.	89
Heavy Metal Emissions (Copper)	Cu	Evaluated the real-time monitoring capability for Cu emissions, highlighting the potential and challenges of direct field measurements; detection limits for lab and in-situ settings were comparable at 15 μg/m3 and 20 μg/m3, respectively.	90
Electronic Waste (E-waste)	Cu	Proved that LIBS serves as a viable alternative technology for monitoring copper leaching processes in electronic waste.	91
Plastic Waste	Cu	Demonstrated the potential of LIBS technology for monitoring copper concentrations within plastic waste streams.	92
Exhaust Gas	Xe, Kr, Cs, Rb	Applied LIBS to monitor elemental flows in Molten Salt Reactor (MSR) exhaust; Partial Least Squares (PLS) processing yielded a prediction confidence interval of 99.9%.	93
Exhaust Gas	Xe, Kr	Evaluated LIBS performance in MSR exhaust monitoring under Ar and He atmospheres; Ar provided higher plasma temperatures, and both atmospheres yielded high model prediction accuracy.	94
MSR Effluents	Hydrogen Isotopes	Developed a multivariate model for quantifying isotopic ratios; after correction, the required calibration sample volume was reduced to 18% of the original, demonstrating real-time MSR effluent monitoring.	95
Exhaust Gas	Hydrogen Isotopes	Showed that LIBS can effectively provide physical insights into gas-salt interactions within MSR systems.	96
Wastewater	Pb, Zn, Ni, Cd, Cr, Co	Monitored heavy metal removal in wastewater, investigating the effects of bentonite type and adsorbent dosage on adsorption efficiency; results were validated by ICP-MS with high consistency.	97
Wastewater	Fe	Performed continuous 10-day LIBS elemental analysis on wastewater from a historical building; combined PCA and LDA for classification, with successful validation via ICP-MS.	98
Recycled Concrete Aggregate (RCA)	---	Integrated LIBS with 3D scanning for online analysis of contaminants in RCA from demolition waste, significantly improving detection precision.	99
Wood Waste	As, Ba, Cd, Cr, Cu, Hg, Pb, Sb, Ti	Employed a multi-line approach (1-3 spectral lines per element) to facilitate the detection of low-sensitivity elements, successfully identifying three categories of contaminated wood waste.	100

first introduced LIBS to laser cleaning. Their study investigated samples such as heavily encrusted sandstones and medieval stained glass. By employing a grating spectrometer and an optical multichannel analyzer, they obtained spectra revealing elemental variations within the samples. Additionally, they designed an experimental setup for laser cleaning to evaluate the potential of LIBS for closed-loop control during the cleaning process. Following this, Fortes *et al.*[104] developed and assessed an orthogonal double-pulse (DP) LIBS configuration in which one laser was used for cleaning metallic artworks, whereas the second served as the LIBS source for analyzing ablated material. Their results demonstrated the feasibility of LIBS for real-time monitoring in metal artwork restoration.

Subsequently, Khedr *et al.*[105] explored the use of plume imaging to monitor the laser cleaning of stone surfaces. In their experiments, high-energy laser pulses were applied to remove crusts from marble substrates, and LIBS was successfully used to analyze the layered structure of the cleaned surfaces.

Sun's team[106] designed an online LIBS monitoring system for real-time evaluation of laser cleaning quality. This system

determined cleaning speed, assessed cleaning effectiveness, and identified the optimal number of ablations passes, thereby providing a foundation for automated control. The team employed mean smoothing for background removal and the DBSCAN algorithm for spectral data processing, thereby effectively reducing errors. They later applied this LIBS system[107] to monitor the laser cleaning quality of carbon fiber reinforced polymers (CFRP), successfully acquiring spectral data of epoxy resin and matrix carbon fibers. By calculating optimal cleaning parameter thresholds, they classified the cleaning quality into three categories: under-cleaning, optimal cleaning, and over-cleaning. These results provide a practical approach for evaluating cleaning effectiveness, optimizing automated control, and classifying cleaning quality.

Li *et al.*[102] developed a LIBS-based system for real-time monitoring of the laser cleaning of hot-rolled stainless steel. They employed the relative intensity ratio (RIR) of Fe II 520.9 nm and Cr II 589.2 nm emission lines as a quantitative indicator to determine optimal cleaning parameters and control cleaning effects by tracking changes in the signal index. Their findings revealed that spectral intensity values increased significantly once oxide layers were removed, while high RIR values persisted under over-cleaning conditions.

Voznesenskaya *et al.*[108] investigated online monitoring of laser cleaning on aluminum alloy surfaces using LIBS. Their spectral analysis identified correlations between treatment modes and cleaned thicknesses, optimal spectral ranges for analysis, spectral lines for coating element comparison, and suitable laser irradiation parameters. Similarly, Li's team[109] employed LIBS to evaluate the removal of epoxy resin coatings from carbon fiber boards by analyzing plasma spectra during the cleaning process. Lei *et al.*[110] focused on real-time monitoring of marine biofilm layers on aluminum alloy surfaces using nanosecond pulsed laser cleaning. Their LIBS results were compared with EDS measurements, yielding errors between 0.9% and 3.8%. Xu's team[111] combined image binarization, area extrapolation, and LIBS to monitor and control soot removal from white marble surfaces. Image binarization was used to establish fixed pulse widths for cleaning, while LIBS simultaneously evaluated cleaning quality. Results confirmed LIBS's ability to remove soot layers caused by human activity without damaging the marble surface.

In the field of laser cleaning, laser-based layered paint removal for aircraft skin has emerged as a prominent research focus within the field of laser processing. This process is typically employed during aircraft maintenance or overhaul to completely strip old paint layers, inspect and repair potential damage to the skin substrate, and prepare the surface for repainting. As aircraft represent one of the most critical instruments driving global economic growth and transportation, effective paint removal is essential for maintaining the integrity of the aircraft skin, extending service life, and ensuring flight safety[112,113].

Since 2021, Yang's team[114–116] have conducted real-time LIBS monitoring of paint removal from aluminum alloy substrates, primers, and aircraft skin topcoats. Their findings revealed that variations in the Ca I 442.7 nm signal served as an indicator of topcoat and primer removal, while changes in the Al I 394.5 nm and 396.2 nm spectral lines provided a basis for evaluating potential damage to the aluminum alloy substrate. Subsequently, they successfully developed a custom-built LIBS monitoring platform for paint removal and integrated machine learning to establish monitoring criteria. Using spectral data from the topcoat, primer, and substrate, they constructed a classification model based on the random forest algorithm, achieving a classification accuracy of 98.89%[115]. In a subsequent study, the same team applied Principal Component Analysis (PCA), Partial Least Squares Discriminant Analysis (PLS-DA), and Orthogonal Partial Least Squares Discriminant Analysis (OPLS-DA) to establish data classification and identification models for testing the LIBS platform. The OPLS-DA model achieved a root mean square error of prediction (RMSEP) of 0.2873, with prediction accuracies of 94.4% for both characteristic spectral lines and full-spectrum data[116]. More recently, they developed a LIBS-based paint removal thickness monitoring model using the standard curve method combined with a Principal Component Analysis–Support Vector Regression (PCA-SVR) algorithm. This model also demonstrated high detection accuracy[117].

These experiments provided core technical support and methodological validation for the application of LIBS in laser-controlled layered paint removal for aircraft skins. The technology offers advantages such as minimal substrate damage and precise measurement capabilities, and thus shows substantial potential for further development in this domain. Compared with the extensive research on aircraft skin paint removal, studies addressing paint removal in other contexts remain relatively limited.

In 2019, Zhou *et al.*[118] analyzed the time-resolved characteristics of paint and spectra during laser paint removal using a monochromator and a photomultiplier tube (PMT). They fitted the time-resolved signals using a double-exponential function and monitored paint removal in real time by tracking the ratio of short- to long-lifetime coefficients (A_{short}/A_{long}), ultimately achieving a cost-effective and efficient cleaning outcome. Subsequently, ShangGuan *et al.*[119] identified zinc and iron spectral lines as indicators of paint removal using LIBS, and employed the K-nearest neighbor (KNN) algorithm to assess the degree of cleaning. This approach not only enabled real-time evaluation of surface cleanliness but also provided information regarding residual paint through the integration of spectral data and algorithmic analysis.

Choi *et al.*[120] utilized a high-power laser to remove thick paint coatings from stainless steel (SS304L) and employed LIBS to assess cleaning effectiveness. They developed a data processing

Table 6. The contributions of various studies in the field of LIBS for real-time monitoring of laser cleaning

Material	Contributions	Refs
Original sandstone and medieval stained glass samples	Introduced LIBS into the field of laser cleaning monitoring for the first time, validating the potential of LIBS-based devices for closed-loop control in cleaning processes.	103
Metallic artworks	Developed an orthogonal double-pulse LIBS (DP-LIBS) system, where one pulse performs the cleaning and the second provides monitoring. The optimization and evaluation of LIBS for the restoration and preservation of metallic artifacts were conducted in this study.	104
Marble substrates	Investigated the stratified structure of cleaned surfaces using LIBS; developed a plume imaging system conducive to monitoring the cleaning process of archaeological lithic artifacts.	105
Carbon fiber composites (CFRP)	Designed a LIBS system capable of determining laser cleaning velocity, evaluating cleaning efficacy, and identifying optimal ablation counts, thereby providing a basis for automated process control.	106
Carbon fiber reinforced polymers	Successfully acquired spectral information on the elemental composition of both the epoxy resin and the carbon fiber matrix; categorized cleaning quality into three distinct levels—insufficient, optimal, and excessive—for quality assessment.	107
Hot-rolled stainless steel	Utilized the relative intensity ratio (RIR) of Fe and Cr emission lines as a quantitative indicator of the cleaning process, controlling cleaning efficacy through real-time monitoring of signal index fluctuations.	102
Aluminum alloys	Determined the relationship between the thickness of the layer to be removed and the processing mode via LIBS spectra, enabling the removal of paint coatings to a specific desired thickness in a single pass.	108
Carbon fiber plates	Monitored the laser cleaning process by measuring the plasma spectra generated during the removal of epoxy resin coatings.	109
Aluminum alloys	Monitored the removal efficacy of marine biofilms on aluminum alloy surfaces using LIBS with nanosecond pulsed lasers; compared with EDS results, the error margin was as low as 0.9%–3.8%.	110
White marble	Employed image binarization to determine the optimal pulse width for laser cleaning, enhancing the safety and reproducibility of removing soot deposition layers from white marble surfaces.	111
Aircraft skin	Analyzed multi-pulse LIBS on aluminum alloy substrates, primers, and topcoats of aircraft skins; demonstrated that variations in spectral intensity or composition serve as indicators of target material removal, showcasing the feasibility of LIBS in aircraft paint stripping.	114
Aircraft skin	Implemented multiple data processing algorithms (RF, PCA, PLS-DA, and OPLS-DA) to establish monitoring models for laser paint removal; classification accuracies for RF and OPLS-DA reached 98.89% and 94.4%, respectively.	115,116
Aircraft skin	Developed paint removal thickness monitoring models based on LIBS spectra using the standard curve method and PCA-SVR algorithms; results indicated that the latter achieved significantly higher precision.	117
Al-based substrates	Analyzed time-resolved characteristics of coatings and spectra using a monochromator and photomultiplier tube (PMT); detected cleaning completion by monitoring the ratio of two experimental coefficients, achieving low-cost and high-efficiency cleaning.	118
Marine steel	Evaluated the degree of laser cleaning using the K-Nearest Neighbors (KNN) algorithm; this approach not only assessed surface cleanliness in real-time but also retrieved the status of residual paint via spectral analysis.	119
Stainless steel	Generated 2D distribution maps using peak intensities of Fe, Cr, and Na LIBS signals; comparison with EPMA results confirmed the reliability and consistency of both methods for monitoring the de-painting process.	120
Carbon fiber reinforced polymers	Employed LIBS combined with a PLS-DA model to monitor paint removal efficacy; the model achieved a classification accuracy of 100%.	121

method to generate two-dimensional distribution maps based on the peak intensities of iron, chromium, and sodium signals. The reliability and consistency of the LIBS approach were confirmed through multivariate analysis of the two-dimensional correlation coefficient distribution, which was validated against results from an electron probe microanalyzer (EPMA).

Zhao *et al.*[121] integrated LIBS with a Partial Least Squares Discriminant Analysis (PLS-DA) model to monitor laser paint removal from carbon fiber reinforced polymer (CFRP) surfaces. Their model achieved a classification accuracy of 100% for assessing paint removal effectiveness, demonstrating the strong potential of LIBS for high-quality surface cleaning and automated applications.

To conclude, LIBS technology has been successfully implemented across a diverse range of laser cleaning scenarios,

extending from the restoration of cultural heritage and industrial metal decontamination to the precise paint removal from aerospace skins. By identifying variations in characteristic emission line intensity ratios (RIR) and integrating sophisticated algorithms such as DBSCAN, Random Forest, and PLS-DA, researchers have achieved not only accurate classification of cleaning levels but also significant enhancements in the response speed of closed-loop control systems. Table 6 summarizes representative cases of LIBS-based cleaning quality monitoring from recent years, categorized by the target cleaning materials and their primary research contributions.

Real-time Monitoring of Laser Materials Processing. Initially, in 2004, Tong *et al.*[122] proposed a real-time feedback control system for ultrafast laser micromachining based on LIBS. Their work highlighted the unique advantages of LIBS-based feedback systems in process monitoring, specifically by minimizing substrate damage, shortening processing times, and achieving superior uniformity in fabricated features. Subsequently, Song *et al.*[123] integrated LIBS with the support vector regression (SVR) method, utilizing processing parameter-conditioned kernel functions to achieve real-time prediction of compositions independent of processing conditions. By employing spectral line intensity ratios and integrated spectral intensities for SVR training, they conducted comparative composition measurements against the calibration curve method, partial least squares regression (PLSR), and artificial neural networks (ANN). Furthermore, SVR demonstrated distinct advantages in addressing non-linear problems; the combination of LIBS and SVR enables the maintenance of accurate real-time predictive performance under fluctuating operating parameters and offers a broader prediction range.

Laser welding represents a critical component of the laser material processing domain. Within this sector, LIBS has emerged as a pivotal tool for diagnosing welding quality and operation modes. For instance, in 2009, Jandaghi *et al.*[124] conducted a theoretical investigation into the compositional variations of weld metal during aluminum alloy welding in keyhole mode, which was subsequently validated through experimental LIBS analysis. The experimental setup is illustrated in Fig. 6. Their study revealed a linear increase in magnesium loss as the duration of the laser welding pulse extended; furthermore, variations in magnesium traces were found to be negligible when the laser power density was altered. A year later, the same research group integrated LIBS with Energy Dispersive X-ray (EDX) and Particle Induced X-ray Emission (PIXE) to analyze pulsed laser welding of stainless steel and aluminum alloys in keyhole mode. While EDX and PIXE were utilized to determine the concentrations of iron (Fe), chromium (Cr), nickel (Ni), and manganese (Mn) within the melt pool, LIBS provided real-time measurements of aluminum (Al) and Mg concentrations. The results indicated a decrease in Mg concentration alongside an increase in Al concentration within the

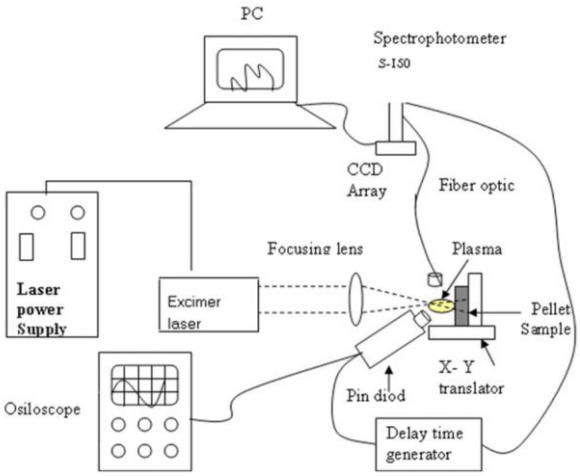

Fig. 6 Typical LIBS experimental setup for laser welding process monitoring (adapted from [124]).

weld metal during the process. Furthermore, while the Al/Mg concentration ratio remained largely unaffected by varying laser power densities, it exhibited a significant correlation with pulse duration[125].

Lednev *et al.*[126,127] performed a detailed exploration of the influence exerted by different weld regions (e.g., the melt pool and solid weld seam) on LIBS signals and plasma characteristics, while concurrently investigating the impact of various laser welding parameters on LIBS measurements. The experiments confirmed that higher surface temperatures in the melt pool led to more pronounced LIBS signal intensities and plasma temperatures; conversely, during defective welding, the acquired signal intensity increased but exhibited diminished stability. Additionally, the characteristics of nanosecond ablation and LIBS plasma were found to be influenced by the welding plasma, resulting in an enhancement of ionic line intensities. This study successfully validated the capability of LIBS to detect defective laser welding and distinguish between different welding modes.

To achieve real-time diagnostics of laser welding processes for diverse aluminum alloys, Maslov and coworkers[128] proposed an optical diagnostic method based on LIBS to monitor the formation of heterogeneous materials and constructed a corresponding apparatus. This system records the spectra of the gas plasma plume generated on the metal surface under laser radiation, which reflects the atomic and molecular evaporation processes within the melt pool. By detecting AlO molecular bands, the presence of surface oxide films can be identified, allowing for the characterization of their destruction under laser radiation and the subsequent monitoring of the welding progress.

More recently, Lukas *et al.*[129] applied calibration-free LIBS (CF-LIBS) for spectral acquisition during gas tungsten arc

welding of duplex stainless steel (GTAW DSS). The results showed a strong correlation with data obtained via partial least squares (PLS) regression, confirming the suitability of CF-LIBS for preventing the formation of weld defects. Furthermore, Yoo *et al.*[130] implemented a LIBS configuration coaxially aligned with a high-power continuous-wave (CW) welding laser, enabling the real-time acquisition of plasma emission signals during the laser welding of copper-steel dissimilar metals. The Cu/Fe emission intensity ratio extracted from the LIBS signals served as the criterion for welding quality assessment. A key advantage of this setup is its seamless integration into existing laser welding systems without the need for additional excitation sources or complex instrumentation, further underscoring the inherent flexibility of LIBS instrumentation.

In parallel, Shangguan *et al.*[131] investigated the relationship between ablation morphology and physical behavior in femtosecond laser-induced plasmas under varying parameters. Their findings revealed that higher laser fluences lead to more intense spectral radiation, increased plasma plume densities, extended lifetimes of ionized particles, and larger ablation craters. The study also identified temperature and electron density as pivotal factors in plasma evolution, thereby validating the feasibility of using LIBS for the online monitoring of laser processing. During the same period, Hongbin *et al.*[132] proposed a LIBS application scheme integrated with a feedback loop system, achieving real-time detection and dynamic decision-making during the laser processing cycle. Furthermore, they implemented an automated material segmentation function within three-dimensional images generated through continuous laser processing.

Recently, Jang's team[133] utilized LIBS in high-resolution laser processing of multilayer films at femtosecond timescales to predict interface positions during laser ablation. They proposed a method to identify interface positions from single LIBS spectra, significantly improving efficiency compared with prior approaches requiring averaged spectral data.

In summary, LIBS technology has extensively permeated various dimensions of laser processing, ranging from the online focal length correction of femtosecond laser micromachining to the coaxial assessment of dissimilar metal welding quality, demonstrating exceptional monitoring precision and integration flexibility. By analyzing plasma plume dynamics and establishing real-time feedback loops, researchers have significantly enhanced the controllability and consistency of the manufacturing process. Table 7 provides a comprehensive summary of the aforementioned literature, categorized by processing materials and their respective research contributions.

Conclusions. This section provides a systematic review of the application progress of LIBS technology in the process monitoring of laser cleaning and laser materials processing. Overall, LIBS demonstrates immense potential for quality control and process automation in advanced manufacturing, primarily due to its distinct advantages, such as eliminating the need for sample pretreatment, enabling simultaneous multi-element characterization, providing in-situ real-time response, and possessing exceptional environmental adaptability.

However, as discussed in the preceding chapter, certain limitations of LIBS persist. For instance, in laser cleaning applications, accurately determining the cleaning threshold and identifying interfacial compositions remain challenging due to the complexity of matrix effects and the plasma shielding effect of the ablation plume on spectral signals. Regarding laser welding monitoring, the inherent instability of the melt pool plasma can lead to a reduction in the signal-to-noise ratio (SNR) of LIBS signals, thereby compromising detection accuracy.

To address these issues, researchers have pursued two primary strategies. On one hand, various methods should be employed to mitigate matrix effects, such as conducting measurements within inert gas environments, including Argon (Ar) or Helium (He)[93]. On the other hand, enhancing measurement stability remains a critical objective. For example, the team led by Inseok J.[133] developed a positioning method capable of online interface prediction, thereby enhancing the precision of sample detection.

ONLINE ENVIRONMENTAL MONITORING

In contemporary society, characterized by rapid economic and technological development, environmental pollution remains a major challenge for both governments and the public. Industrial production is a particularly significant contributor to environmental degradation, as excessive emissions of carbon dioxide, methane, and sulfur dioxide from exhaust gases lead to severe atmospheric pollution, while wastewater containing heavy metals, organic pollutants, and other hazardous substances results in water and soil contamination[11,134,135]. As these environmental problems intensify, there is an urgent need for systematic research aimed at reducing pollutant emissions and controlling the release of toxic substances. Laser-induced breakdown spectroscopy (LIBS), as an advanced real-time monitoring tool, has emerged as an important technique for addressing these pressing environmental concerns. Its applications in environmental monitoring are discussed in detail below.

Monitoring of atmospheric pollutants. Atmospheric pollutants include PM2.5, PM10, sulfur dioxide, carbon monoxide, and other gaseous pollutants or particulate matter. Aerosols, defined as solid or liquid particles suspended in the air, originate from direct

Table. 7 The contributions of various studies in the field of LIBS for real-time monitoring of laser materials processing

Material	Contributions	Refs
Micro-heaters	Successfully fabricated micro-heater structures on thermal spray materials using LIBS-controlled micromachining, demonstrating the feasibility of closed-loop feedback control in laser materials processing.	[122]
Titanium and Aluminum Metals	Combined LIBS with Support Vector Regression (SVR) and compared it with Artificial Neural Networks (ANN) for compositional measurement, demonstrating the superior performance of SVR in resolving nonlinear issues.	[123]
Aluminum Alloy	Conducted theoretical and experimental LIBS validation of weld metal compositional variations during keyhole-mode welding, identifying the evolutionary patterns of magnesium.	[124]
Aluminum Alloy and Stainless Steel	Characterized the concentration trends of magnesium and aluminum in weld metals during laser welding using a combined methodology of LIBS, EDX, and PIXE analysis.	[125]
Inconel 718 Alloy	Investigated the influence of different weld regions (molten pool vs. solid weld) and laser welding process parameters on LIBS signals and plasma characteristics; successfully validated the capability of LIBS to detect welding defects and distinguish between welding modes.	[126,127]
Various Aluminum Alloys	Proposed an optical diagnostic method based on LIBS for the formation process of heterogeneous materials and constructed a corresponding apparatus; the system recorded plasma plume spectra on metal surfaces under laser radiation to characterize atomic and molecular evaporation in the molten pool.	[128]
Duplex Stainless Steel	Confirmed the applicability of Calibration-Free LIBS (CF-LIBS) for preventing weld defect formation within Gas Tungsten Arc Welding (GTAW) environments.	[129]
Copper and Steel	Enhanced LIBS technology using a coaxial optical configuration aligned with a high-power continuous-wave (CW) welding laser; the setup integrates easily into existing laser systems without additional excitation sources, demonstrating the high flexibility of LIBS instrumentation.	[130]
Sapphire	Revealed the plasma evolution process during sapphire laser processing, verifying the feasibility of LIBS for the online monitoring of laser machining.	[131]
Aluminum, Silicon, Titanium, and Copper Samples	Described a LIBS-based feedback loop system for real-time monitoring and dynamic decision-making during laser processing, with the capability to generate material distribution maps for subsequent analysis.	[132]
Aluminum Thin Films	Proposed and validated a high-efficiency method for determining machining interface positions based on a single LIBS spectrum.	[133]

emissions (*e.g.*, dust, black carbon) or secondary formation through gas-to-particle conversion (*e.g.*, sulfates, nitrates). In addition to directly reducing air quality and visibility, aerosols significantly impact climate change by influencing cloud formation and radiative forcing[136].

In 2001, Carranza *et al.*[137] employed LIBS for monitoring aerosols in ambient air, reporting six weeks of real-time data on aerosols containing aluminum, calcium, magnesium, and sodium. Aerosol particles ranging from 100 nm to 2 μm in diameter were successfully measured, achieving detection limits on the order of milligrams per cubic meter (e.g., mg/m³). Subsequently, Hettinger *et al.*[134] examined correlations between LIBS monitoring of specific and non-specific aerosols through statistical analyses of airborne particles, reporting significant correlation coefficients (R^2 values ranging from 0.22 to 0.93) for aerosols sampled within the 500 nm–2.5 μm range. This study also demonstrated the high temporal resolution of LIBS by capturing aerosol fluctuations on a 5–10 min timescale. Similarly, Gallou *et al.*[138] conducted real-time monitoring of pollutants, including heavy metals, emitted from industrial exhaust stacks to improve air quality. They compared two primary laser focusing approaches: indirect analysis of particles collected on filters and direct aerosol analysis. While indirect analysis yielded greater effectiveness, direct analysis achieved superior detection limits of 15 μg/m³ compared with 60 μg/m³ for the indirect method.

To overcome the detection limit bottlenecks caused by sparse aerosol sampling, in 2013, Diwakar 's team[139] proposed a novel method for near real-time aerosol particle analysis. Their approach involved electrostatic deposition of charged particles onto flat-tipped microneedle electrodes, allowing pre-concentration of particle mass directly from the aerosol stream. The collected material was subsequently ablated and analyzed via LIBS. Detection limits for Cr, Cd, Cu, and Mn were in the range of 0.018–5 ng. This electrostatic collection method offered enhanced accuracy compared with conventional techniques and provided valuable guidance for the development of compact portable LIBS instruments.

Subsequently, Tjärnhage *et al.*[140] developed a pulsed laser LIBS system for detecting aerosolized biological warfare agents (BWAs), significantly improving single-particle detection rates. Specifically, hit rates for 3 μm and 7 μm sodium chloride particles increased from 1% and 2% using traditional methods to 40% and 70%, respectively.

Under extreme industrial environments, the team led by Girón's team[141] demonstrated a dual-pulse LIBS system with a sampling distance of up to 8 meters. This system successfully identified aerosol particles containing elements such as chromium, hypothesized to originate from casting powders removed during oxygen cutting of stainless steel slabs. Despite a particle sampling rate below 6%, elemental characterization was achieved using robust statistical methods, demonstrating LIBS as a viable tool for controlling particulate emissions in harsh industrial environments.

In 2019, Kim *et al.*[142] investigated the sensitivity of LIBS for detecting various aerosol elements generated in laboratory settings, successfully observing emission lines for P, Fe, Mg, Cu, Co, Ni, Ca, Na, and K. Additionally, Qu *et al.*[143] conducted an in situ LIBS study using smoke from burning mosquito repellent incense as an example of localized air pollution monitoring. Their findings indicated that human respiratory gases contained additional C, H, and CN molecular bands, while characteristic peaks for Fe, Ca, Ti, Sr, and Cr—major contributors to atmospheric pollution—were observed in the smoke. Similarly, He *et al.*[144] simulated uranium emission monitoring during nuclear accidents using LIBS and successfully tracked spectral line intensity variations associated with the emission and deposition of UOx particles in aerosols.

Wan's team[145] applied LIBS to the real-time detection of soot in various coal combustion processes, monitoring elements such as Al, Fe, Ca, and CN molecular bands. Combining PCA for dimensionality reduction with a back-propagation artificial neural network (BP-ANN), they achieved predictive accuracies exceeding 92%. They further integrated LIBS with a Single Particle Aerosol Mass Spectrometer (SPAMS) to analyze indoor pollutants generated during electronic soldering, identifying lead and tin as the primary components and performing real-time monitoring of indoor carbon concentrations[146]. These findings demonstrated the applicability of LIBS for monitoring both combustion emissions and indoor air pollutants.

Prüfert *et al.*[147] presented an integrated platform combining LIBS, laser-induced incandescence (LII), and additional techniques for the quantitative and qualitative monitoring of industrial aerosols, representing the first instance of such laser irradiation technologies being used for online real-time aerosol analysis. Their method employed a coefficient of variation (CV)-based approach utilizing photodiodes and microphones for partial photoacoustic normalization of spectral intensities, reducing CV by up to 25%. A secondary laser for LII successfully classified particles based on incandescence trends. Han B. et al.[148] focused on detecting carbon during combustion, using a LIBS system to identify C atomic lines and CN and CaO molecular bands across charcoals with varying combustion levels. They implemented SVM, RF, CNN, and other models, optimized SVM hyperparameters using particle swarm optimization (PSO), and applied PCA and LDA for spectral feature extraction and dimensionality reduction. Their LDA-PSO-SVM calibration model yielded an RMSEP of 0.035% and an MRE of 3.877%.

In 2025, Aizezi *et al.*[149] utilized LIBS for real-time analysis of fumes generated during welding, demonstrating that rising temperatures promote lead and tin evaporation while significantly increasing carbon spectral intensity, with Pearson correlation coefficients exceeding 0.8 for temperature versus spectral intensities. Concurrently, Ye *et al.*[150] proposed an optimized machine learning method combining Kernel Principal Component Analysis (KPCA) and Random Forest (RF) to analyze industrial smoke particles using single-particle aerosol mass spectrometry, achieving an R^2 of 0.843 on the test set. Huang *et al.*[151] deployed LIBS in a classroom setting to monitor changes in airborne particulate matter concentrations attributable to chalk dust.

Collectively, these studies highlight the broadening scope of LIBS for air pollutant monitoring. They not only underscore LIBS's analytical potential in real-world contexts but also reinforce its relevance in addressing the associated health risks, thereby offering a practical basis for air pollution monitoring and mitigation. In conclusion, Table 8 summarizes the research contributions presented in this chapter, categorized by monitoring scenarios, target elements, and their corresponding limits of detection.

Water Quality Monitoring. In 1997, Smith [152] demonstrated the potential of laser-induced breakdown spectroscopy (LIBS) probe devices for elemental analysis in aqueous media. The study evaluated five plasma generation methods for LIBS fiber optic probes and identified a superior and practical approach, highlighting the significant commercial potential of LIBS for real-time water flow monitoring.

Hartzler *et al.*[153] developed a LIBS-based sensor designed to monitor water sources for contamination by dissolved metals originating from subsurface brines or formation rocks. Their system exhibited strong performance in terms of calibration curve linearity, sampling speed, and detection limits for target elements. The fiber-coupled design of the LIBS device separated the laser, pump source, and spectrometer, thereby allowing sensitive and costly components to remain safely at the surface. This configuration reduced equipment costs and enhanced operational feasibility in harsh downhole water conditions, thus improving the device's cost-effectiveness for field applications.

Table. 8 The contributions of various studies in the field of LIBS for monitoring of atmospheric pollutants

Monitoring Scenario	Analyte Elements or Compositions	Contributions	Refs
Outdoor atmosphere	Ca, Mg, Na, Al	Achieved sub-picogram absolute mass detection limits for single-particle analysis; confirmed that LIBS can resolve challenges associated with real-time collection and analysis of ambient air particulate data.	137
Outdoor atmosphere	Ca, Na, Al	Elucidated the correlation between specific and non-specific aerosol monitoring; demonstrated that LIBS technology possesses high temporal resolution.	134
Chimney exhaust gas	Cu	Applied LIBS for online monitoring of heavy metals (Cu) in gaseous particulates; found that indirect analysis is more effective while direct analysis offers superior detection limits.	138
Outdoor atmosphere	Cd, Cr, Cu, Mn, Na, Ti	Developed a novel method for collecting airborne particles at the tip of a microneedle for LIBS aerosol monitoring; achieved detection limits superior to concurrent ICP-AES.	139
Aerosolized biological warfare agents	Biological warfare agents (BWA)	Utilized LIBS for compositional monitoring of BWAs; significantly improved particle hit rates and enhanced the accuracy of the identification process.	140
Industrial production aerosols	Cr, Ca, Al, *etc.*	Evaluated and confirmed the robust analytical performance of LIBS equipment for aerosols under the harsh environments of steel production.	141
Laboratory aerosols	P, Fe, Mg, Cu, Co, Ni, Ca, Na, K	Evaluated and validated the multi-element simultaneous detection capabilities of the developed Aerosol-LIBS system.	142
Mosquito coil smoke	Fe, Ca, Ti, Sr, Cr, Mn, Pb, C, H, and CN molecular bands	Performed in-situ LIBS monitoring of air pollution using mosquito coil smoke as a case study and successfully detected relevant elements.	143
Uranium aerosols from nuclear accidents	U	Demonstrated the potential of LIBS for emergency response in nuclear accidents and continuous monitoring of uranium aerosol emissions.	144
Coal combustion smoke	Al, Fe, Ca, etc., and CN molecular bands	Combined LIBS with PCA dimensionality reduction and BP-ANN model classification, achieving an identification accuracy exceeding 92%; confirmed the viability of LIBS for soot detection and identification.	145
Welding fumes and indoor atmosphere	Pb, Sn, C	Integrated LIBS with SPAMS to detect indoor air pollutants caused by electronic welding operations; conducted online monitoring of indoor carbon concentrations.	146
Industrial production aerosols	Aluminum-containing and copper-containing particles	Employed LIBS, Laser-Induced Incandescence (LII), and other instruments to monitor industrial aerosols; introduced a method capable of reducing the coefficient of variation to 25%.	147
Charcoal combustion smoke	C, CN molecular bands, and CaO molecular bands	Evaluated PLS, SVM, RF, and CNN models and utilized the PSO algorithm to optimize SVM hyperparameters; results indicated that the LDA-PSO-SVM model performed best.	148
Welding fumes	Pb, Sn	Demonstrated that increased temperatures during welding promote the evaporation of lead and tin in fumes; observed a clear upward trend in the intensity of carbon spectral lines.	149
Welding fumes	Sn, Pb, C, H, *etc.*	Utilized KPCA for non-linear dimensionality reduction of mass spectrometry data combined with RF for prediction; provided an effective method for precise aerosol or smoke particle identification.	150
Indoor atmosphere	Ca, K, Mg, N, O, *etc.*	Applied a LIBS system for the first time in a classroom environment to monitor aerosol variations derived from traditional chalk dust.	151

However, direct LIBS detection of liquids often suffers from a significant reduction in measurement precision due to phenomena such as liquid splashing and plasma quenching; consequently, to address these issues, Jiang *et al.*[154] developed a micro-gas-column-assisted LIBS (MGC-LIBS) system for in situ bulk water analysis, reducing the detection limit for magnesium by nearly sixfold while achieving relative standard deviations ranging from 0.12% to 11.51%.

Subsequently, Sui *et al.*[155] introduced an online ultrasonic nebulizer-assisted LIBS (OUN-LIBS) system for detecting and analyzing metal elements in seawater. Based on the operational principle of this sensor, they constructed a hardware platform comprising three modules: water sample atomization, LIBS detection, and communication control, complemented by a software system featuring a fully integrated online monitoring

program. By atomizing liquid samples into aerosols for LIBS analysis, the device successfully detected six metal elements in seawater under continuous monitoring conditions, achieving detection limits below 1 ppm and stability values under 0.38%. This OUN-LIBS system demonstrates substantial research value and promising prospects for applications in marine environmental monitoring and marine science research. Luo *et al.*[156] combined one-point calibration laser-induced breakdown spectroscopy (OPC–LIBS) with aerosolization techniques to achieve high-precision, rapid quantitative analysis of water hardness. Their results demonstrated that the average relative errors for Ca, Mg, and Sr measured by this method were consistently lower than those obtained via internal and external standard methods.

In response to signal fluctuations induced by droplet splashing, Xiong's team[157] advanced this field by implementing a tip-enhanced LIBS method, wherein high-temperature plasma is generated by pre-exciting a metal tip before ablating the atomized solution. This approach effectively suppressed signal instability caused by droplet splashing and plasma quenching during liquid detection, significantly improving measurement performance near the detection limit. The technique was further enhanced through the application of Gaussian Process Regression (GPR) modeling, which amplified spectral intensities for the elements of interest. Using this method, detection limits for copper, manganese, and chromium were all achieved at approximately 50 mg/L.

More recently, Andrews's team[158] employed LIBS to perform in-situ, real-time quantitative detection of elemental impurities using an engineered sampling system that forms a thin liquid layer on a rotating wheel. Eight elements, including Na, Al, and K, were successfully measured, and univariate and multivariate calibration yielded the best detection limit of 53.2 mg/L.

In another study, LeCroy *et al.*[159] demonstrated the effectiveness of LIBS for real-time monitoring of neodymium and praseodymium concentrations in flowing aqueous solutions. Their system achieved root-mean-square prediction errors (RMSEPs) of 0.15 mol/L and 0.21 mol/L, respectively, confirming its predictive stability.

To further improve detection precision, recently, Wang *et al.* [160] employed a combination of electrodeposition (ED) and spark discharge-assisted laser-induced breakdown spectroscopy (SD-LIBS) for the high-sensitivity detection of Cr in water, achieving a limit of detection (LOD) as low as 1.19 μg/L. Furthermore, Wang *et al.* [161] constructed a compact spectral acquisition system integrating a micro-spectral sensor with ultra-narrowband filters. By optimizing the optical configuration, they significantly reduced the device footprint and cost while maintaining excellent detection sensitivity for various elements in water bodies, with the LOD for certain elements reaching only 26.9% of that of traditional systems.

In conclusion, these studies underscore the potential of LIBS for real-time, online monitoring of hazardous and trace elements in aqueous solutions. However, most experiments reported detection limits at the mg/L level, whereas, according to current drinking water safety standards and industrial wastewater discharge regulations, metal element concentrations are typically in the μg/L range. This indicates that further improvements in LIBS sensitivity are necessary for it to meet these stringent requirements. Nonetheless, due to its inherent advantages of real-time and in situ monitoring, LIBS retains strong prospects for future applications in water quality analysis. Table 9 summarizes the detected elements, limits of detection (LOD), and primary research contributions of the aforementioned literature regarding water quality analysis.

Elemental monitoring of soil pollution. In 2011, Marcella *et al.*[162] employed LIBS to analyze soil samples from various sources, focusing on five heavy metals: chromium, copper, lead, vanadium, and zinc. They plotted LIBS data against the results obtained from inductively coupled plasma optical emission spectrometry (ICP-OES) and conducted a comparative analysis. The findings demonstrated strong agreement between ICP-OES and LIBS, providing preliminary confirmation of the effectiveness of LIBS for monitoring soil pollutants.

Concurrently, Amina *et al.*[163] addressed the need for time-efficient, low-cost, and rapid soil pollution analysis by developing an online LIBS device capable of directly delivering semi-quantitative information. This device was applied to assess contamination levels in a region of France with elevated heavy metal concentrations. After testing, the results revealed a strong correlation between pollutant concentrations inferred by LIBS and those determined using inductively coupled plasma atomic emission spectroscopy (ICP-AES). The detection limits achieved were 200 ppm for Pb and 80 ppm for Cu. In addition, Meng *et al.*[164] developed a LIBS instrument for heavy metal analysis in soils and compared its performance with that of inductively coupled plasma mass spectrometry (ICP-MS). Their results also showed good consistency, providing experimental validation and practical support for the use of LIBS in the rapid, in-field detection of soil heavy metals.

In recent years, to address matrix effects and stability issues in soil analysis, researchers have significantly enhanced the detection capabilities of LIBS systems by optimizing optical configurations or introducing auxiliary material-based methods. In 2024, for instance, Li *et al.*[165] first applied Confocal-Controlled Laser-Induced Breakdown Spectroscopy (CCLIBS) to the quantitative analysis of heavy metal cadmium (Cd) in soil. The study demonstrated that, compared to conventional LIBS, CCLIBS offers superior spatial consistency and stable plasma temperatures, thereby enhancing detection stability. By employing Partial Least Squares (PLS) to establish a predictive model, the researchers achieved robust results, with an R^2 of 0.96, and RMSEP and ARE

Table 9. The contributions of various studies in the field of LIBS for monitoring of water quality

Elements and LOD	Contributions	Refs
Mg can reach ppm, Na, Ca	Evaluated five breakdown methods for LIBS fiber-optic probes, demonstrating significant commercial potential for real-time water flow detectors.	[152]
Ca 0.10 ppm, Sr 0.04 ppm, K 0.009 ppm	Developed a LIBS monitoring device for detecting groundwater contamination while reducing instrumentation costs for operation under harsh downhole water conditions.	[153]
Mg 0.88 mg/L, Ca 0.35 mg/L, Sr 0.48 mg/L, Na 0.18 mg/L, K 0.36 mg/L, Li 0.13 mg/L	Developed a micro-gas column assisted LIBS (MGC-LIBS) technique for the in-situ analysis of bulk water samples; achieved LODs below 1 mg/L for all target elements.	[154]
Na 0.58 mg/L, Mg 0.38 mg/L, Ca 0.47 mg/L, K 0.95 mg/L, Sr 0.11 mg/L, Li 0.29 mg/L	Developed an online ultrasonic nebulizer-assisted LIBS system for the analysis of metallic elements in seawater; achieved LODs below 1 mg/L under continuous monitoring with stability better than 0.38%.	[155]
Cu 42.80 mg/L, Mn 51.25 mg/L, Cr 58.40 mg/L	Improved detection stability through a unique needle-tip enhancement method and significantly amplified the spectral intensity of target elements using a Gaussian Process Regression (GPR) model.	[157]
Ca 1.41 mg/L, Mg 2.714 mg/L	Applied one-point calibration LIBS (OPC-LIBS) coupled with aerosolization for high-precision, rapid analysis of water hardness; the average relative error was lower than those of conventional internal and external standard methods.	[156]
Na 0.0532 mg/mL, Al 18.5 mg/mL, K 0.105 mg/mL, Ca 0.273 mg/mL, Ti 67.7 mg/mL, Sr 0.640 mg/mL, Mo 22.4 mg/mL, Yb 22.9 mg/mL	Employed LIBS for the in-situ, real-time quantitative detection of elemental impurities using an engineered sampling system that forms thin liquid films on a rotating wheel.	[158]
Nd 0.012 mol/L, Pr 0.020 mol/L	Utilized a LIBS system for the real-time monitoring of neodymium and praseodymium concentrations in flowing aqueous solutions, demonstrating excellent predictive stability.	[159]
Cr 1.19 μg/L	Achieved ultra-sensitive detection of Cr in water using electrodeposition-spark discharge-assisted LIBS (ED-SD-LIBS), reaching μg/L level detection limits.	[160]
Pb 196.18 mg/L, Cu 4.57 mg/L	Constructed a compact spectral acquisition system integrating a micro-spectral sensor and ultra-narrowband filters; the system features a small footprint and low cost while offering higher detection sensitivity for water bodies compared to traditional LIBS.	[161]

values of 67.67 and 0.2, respectively.

Li and colleagues[166] explored the signal enhancement mechanisms of conductive materials, specifically NaCl and graphite, for the quantitative LIBS detection of lead (Pb) in soil. They established univariate and multivariate quantitative analysis models, including Partial Least Squares Regression (PLSR), Least Squares Support Vector Machine (LS-SVM), and Extreme Learning Machine (ELM). The results indicated that the univariate model based on the Pb I 405.78 nm line exhibited the best performance, yielding an R_p of 0.984 and a minimum limit of detection (LOD) of 26.142 mg/kg. In parallel, Fu *et al.*[167] proposed a novel method combining nanoparticle-modified ion exchange membranes with LIBS (NMIEM-LIBS) for monitoring Pb and Cr in soil, achieving LODs for Cd and Pb of only 2.62 mg/kg and 0.24 mg/kg, respectively. Furthermore, the team achieved favorable recovery rates for Pb (87.02–115.79%) and Cd (82.45–114.81%) across three lead-augmented soil samples, fully validating the immense potential of this LIBS technique for heavy metal monitoring and effective element recovery.

Subsequently, Li *et al.*[168] successfully mitigated matrix effects by utilizing dual spectrometers for the collaborative acquisition of spectral information from Cd and the soil matrix. Simultaneously, graphite (C) doping was employed to enhance the spectral intensity of Cd. They also proposed an AWN-Offset Coefficient (O)-LWNet spectral fusion model, which demonstrated excellent predictive performance, reducing the ARE for Cd detection to 7.17%.

Gou *et al.*[169] proposed a laser-induced breakdown spectroscopy approach (Au@SiO_2NPs-SMS-LIBS) integrating Au@SiO_2 nanoparticles with surface microstructures to enable rapid detection of Pb, Cr, and Cu in soils. The method achieved the lowest detection limits (LDLs) of 0.36 mg/kg for Pb, 0.32 mg/kg for Cr, and 0.28 mg/kg for Cu, with relative standard deviations (RSDs) ranging from 5.47% to 6.72%. The inclusion of Au@SiO_2 nanoparticle-based surface microstructures enhanced both the sensitivity and stability of LIBS measurements, while further optimization of the experimental results was accomplished using a stacked modeling approach combining support vector regression (SVR) and partial least squares regression (PLSR).

Recently, Han and colleagues[170] developed a LIBS-based instrument capable of elemental analysis and imaging of contaminated soils. This apparatus enables the visualization of the spatial distribution of heavy metal elements based on characteristic spectral intensities. By employing a K-means clustering algorithm

Table 10. The contributions of various studies in the field of LIBS for monitoring of soil pollutants

Elements and LOD	Contributions	Refs
Cr 17 mg/kg, Cu 61 mg/kg, Pb 20 mg/kg, V 29 mg/kg, Zn 55 mg/kg	Plotted the functional relationship between LIBS data and ICP-OES results; the high consistency observed preliminarily confirmed the effectiveness of LIBS for soil pollutant monitoring.	[162]
Pb 200 ppm, Cu 80 ppm	Designed an online LIBS analytical device providing semi-quantitative information; the results showed high correlation with concentrations inferred by ICP-AES.	[163]
Fe, Si, Al, Ca, Mg, Ti	Developed a LIBS method and apparatus for soil heavy metal analysis and conducted field testing; results demonstrated excellent consistency with ICP-MS measurements.	[164]
Cd 49.06 ppm	Successfully applied CCLIBS for the first time in the detection of heavy metals in soil; the PLS prediction method yielded promising results.	[165]
Pb 26.142 mg/kg	Investigated the enhancement mechanisms of conductive materials (NaCl and graphite) on LIBS signals for Pb in soil and employed multiple prediction models, including ELM, LS-SVM, and PLSR.	[166]
Pb 2.62 mg/kg, Cd 0.24 mg/kg	Adopted a novel NMIEM-LIBS detection method; results exhibited high precision for Pb and Cd detection and achieved effective metal recovery in soil.	[167]
Cd 1.46–3.63 mg/kg	Utilized dual-spectrometer synergistic acquisition of Cd and soil matrix spectral information to mitigate matrix effects; employed graphite (C) doping to enhance spectral intensity.	[168]
Pb 0.36 mg/kg, Cr 0.32 mg/kg, Cu 0.28 mg/kg	Improved detection stability and sensitivity using surface microstructures and Au@SiO_2 nanoparticles; a stacked model of SVR and PLSR further optimized experimental results.	[169]
Cu, Cr, Pb	Developed a LIBS instrument capable of elemental analysis and imaging of contaminated soil, providing a critical basis for environmental monitoring and soil remediation efforts.	[170]

to analyze the spectral data, the soil surface was categorized into heavily, moderately, and lightly contaminated regions. This classification methodology provides a critical foundation for environmental monitoring and subsequent soil remediation efforts.

These research findings demonstrate that the development of auxiliary materials for signal enhancement, as well as the implementation of clustering algorithms for the visualization of contaminated areas, has significantly expanded the application boundaries of LIBS. Table 10 further organizes the specific performance indicators and core technical contributions of various research schemes in soil elemental detection.

Conclusions. In summary, this chapter provides a systematic review of the application progress of LIBS technology in environmental engineering sectors, specifically atmospheric aerosols, water quality safety, and soil contamination monitoring. From the real-time capture of micro-scale particulate matter in ambient air to the in-situ diagnosis of industrial wastewater and deep-well sources, and further to the spatial elemental mapping of heavy metals in contaminated soils, LIBS has demonstrated its capacity to provide critical technical support for establishing integrated land-sea-air environmental early-warning systems. These capabilities stem from its unique advantages, including intrinsic in-situ detection, exceptional temporal resolution, and the ability to simultaneously characterize both organic and inorganic components.

However, in the transition toward large-scale real-time environmental monitoring, LIBS technology still faces significant challenges arising from the complexity of environmental matrices. In atmospheric monitoring, the stochastic diffusion and sparse distribution of aerosol particles limit the effective laser hit rate and the representativeness of sampling. Regarding water quality monitoring, issues such as quenching effects in liquids, splashing interference, and insufficient sensitivity to trace elements present obstacles to meeting the analytical requirements for drinking water safety standards. In the field of soil monitoring, complex matrix effects continue to pose challenges to the stability of quantitative analysis.

To address these limitations, researchers are exploring diversified optimization strategies. On one hand, system improvements at the physical level are being implemented to enhance signal quality; for instance, the team led by Diwakar.[139] utilized electrostatic deposition for particulate pre-concentration, significantly lowering absolute detection limits, while the team of Sui[155] introduced ultrasonic nebulization assistance to effectively overcome detection difficulties in liquid environments. On the other hand, the integration of cross-disciplinary algorithms has opened new avenues for improving predictive accuracy. For example, the team of Han[148]. leveraged multi-model evaluation combined with Particle Swarm Optimization (PSO) algorithms to substantially suppress prediction errors. With the further maturation of compact and intelligent integrated systems, LIBS is

expected to play an indispensable role in the rapid source tracing of accidental environmental pollution events and the comprehensive assessment of ecological remediation processes.

REAL-TIME MONITORING IN OTHER AREAS

In addition to the aforementioned fields of industrial production, laser processing, and environmental optimization, applications for real-time LIBS monitoring have emerged across various other sectors in recent years. For instance, in the field of fundamental manufacturing and processing, Ferioli *et al.*[171] successfully applied LIBS to measure the equivalence ratios of spark ignition engines in laboratory experiments. In their study, the peak elemental ratios of C/N, C/O, and CN/O were used as indicators of equivalence ratios. Their findings suggested that these ratios may be influenced by factors such as pressure variations in the loaded samples and particle size fluctuations within the gas stream. Separately, Zhang *et al.*[172] applied LIBS to monitor cement raw meal quality, improving measurement stability by controlling jet stream powder concentration, laser pulse energy, and other parameters. Zhang *et al.*[173] combined LIBS with near-infrared spectroscopy (NIRS) to analyze key compounds, such as CaO and SiO_2, in cement production. Using a dual-branch convolutional neural network with an attention module (DBAM-CNN), they significantly enhanced LIBS-NIRS data fusion, achieving high-precision detection.

In 2025, Cheng *et al.*[174] integrated LIBS with deep learning and image preprocessing techniques to detect cosmetic defects in ceramic products and successfully monitored key parameters in real time during the sintering process. Similarly, Dong H.'s team[175] employed LIBS to estimate ceramic substrate surface temperatures based on elemental intensity ratios, incorporating machine learning for enhanced accuracy.

In some specialized manufacturing and processing sectors, LIBS technology has also seen substantial development. For instance, Amodeo *et al.*[176,177] employed LIBS for real-time monitoring of nanoparticle production via laser pyrolysis. They successfully observed the Si/Cx allotropic ratio, thereby providing calibration data crucial for nanoparticle synthesis. Their study also indicated that LIBS holds greater potential for monitoring leakage and accidental releases during nanoparticle production than for analyzing individual nanoparticles. Additionally, Alvarez-Llamas *et al.*[178] performed online elemental characterization of nano-aerosols using LIBS in conjunction with an aerodynamic lens system that collimates nanoparticles into focused beams. This approach minimized spectral line broadening and improved spectral resolution. They also monitored the relative elemental composition of Li_2TiO_3 nanoparticles during gas-phase synthesis via laser pyrolysis, highlighting LIBS's potential for nanoaerosol analysis. Jiang X. et al.[179] conducted the first investigation into the effects of laser energy, magnetic fields, and related factors on plasma persistence using LIBS on a linear plasma device (PSI-2).

Beyond the aforementioned fields, the scope of LIBS monitoring technology continues to progressively expand, Cuñat *et al.*[180] utilized a compact, portable LIBS instrument developed in their laboratory to measure lead content in road sediment in real time. The detection limit (LOD) and relative standard deviation (RSD) for lead were 190 μg/g and 9%, respectively, with an approximate 14% deviation when compared to flame atomic absorption spectrometry (AAS). Although the accuracy of this LIBS system has yet to meet regulatory standards, it offers distinct advantages and strong potential for rapid in situ analysis.

Goueguel's team[181] developed a LIBS system capable of producing dissolution curves of calcium carbonate relative to carbon dioxide concentration during underwater measurements. This experiment not only identified the spectral lines of Ca^{2+} and Ba^{2+} in CO_2- saturated water but also established the relationship between Ca^{2+} concentration and CO_2 pressures within the range of 50–350 bar, achieving a detection limit of approximately 5 ppm for Ca^{2+}. This represents an important advance in the real-time monitoring of underwater carbonate dissolution using LIBS.

Lim and Keerthi's team[182] conducted in situ LIBS monitoring of hydroponic nutrient solutions used in crop cultivation, achieving RSD values between 6% and 13% for elements such as K, Na, and Ca. In a subsequent study[183], they proposed an optically modified, direct spectrally coupled LIBS system capable of enhancing hydroponic solution quality monitoring. This automated approach improves the efficiency of nutrient management practices in agricultural settings.

Li *et al.*[184] employed a LIBS system integrated with a solid-liquid-solid-transformation (SLST) protocol to conduct rapid in situ analysis of soil micronutrients. Detection limits for elements such as Cu and Fe met the Chinese classification standards for bioavailable soil elements (Classes I–IV), and the total detection time of 20 minutes underscored the system's efficiency in micronutrient assessment. Zhang *et al.*[185] integrated a LIBS system into a circulating dialysate platform for high-precision electrolyte cation analysis, applying multiple linear regression modeling to align its performance with clinical standards for dialysis monitoring.

Nakanishi's team[186] demonstrated a sensitive technique that combined LIBS with a liquid sheet jet to detect trace precious metals (*e.g.*, Au, Pt, Pd) in acidic aqueous solutions for metal recovery. Using acid-resistant glass slit nozzles to produce liquid sheet jets with thicknesses of tens of micrometers, they enhanced both sensitivity and stability for liquid-phase LIBS measurements, achieving detection limits below 1 mg/L. Building on this,

Table 10. The contributions of various studies in the field of LIBS for monitoring in other areas

Monitoring Scenario	Specific Analyte/Subject	Contributions	Refs
Fundamental Manufacturing & Processing	Engines	Observed that specific elemental peak ratios may correlate with factors such as sample pressure variations and particle size changes in airflows.	[171]
	Cement	Improved measurement stability by stabilizing jet powder concentration and laser pulse power.	[172]
	Cement	Combined LIBS with NIRS and utilized the DBAM-CNN fusion method to enhance spectral signals.	[173]
	Ceramic Manufacturing	Monitored key parameters by integrating LIBS with deep learning and image pre-processing techniques.	[174]
	Ceramics	Estimated surface temperature via elemental intensity ratios, aided by the introduction of machine learning.	[175]
Specialized Manufacturing & Processing	Nanoparticles	Monitored the Si/Cx ratio, providing essential calibration data for nanoparticle production.	[176,177]
	Nano-aerosols	Utilized an aerodynamic lens system to reduce line broadening and improve spectral resolution; conducted online monitoring of relative elemental composition during gas-phase synthesis of Li_2TiO_3 nanoparticles.	[178]
	Plasma Components	Conducted the first investigation on linear plasma equipment using LIBS to study the impact of factors such as laser energy on plasma sustainability.	[179]
Other Fields	Road Sediments	Compared LIBS and AAS results, finding a deviation of approximately 14%.	[180]
	Underwater Calcium Carbonate	Made significant contributions to the real-time monitoring of underwater carbonate dissolution via LIBS.	[181]
	Crop Nutrient Solutions	Achieved detection RSDs for K, Na, and Ca in the range of 6%–13%; proposed an optically modified direct-spectrum coupled LIBS system to enhance the efficiency of farmland nutrient management.	[182,183]
	Soil Nutrients	Integrated LIBS with the SLST protocol; detection limits for Cu, Fe, and other elements met the requirements of Levels I–IV of the Chinese Soil Bioavailable Element Classification Standards.	[184]
	Dialysate	Employed a multivariate linear regression model to meet clinical requirements for monitoring electrolyte cations in dialysate.	[185]
	Acidic Aqueous Solutions	Combined LIBS with liquid-sheet jet technology, achieving detection limits below 1 mg/L for all target elements.	[186]
	Electronic Waste (E-waste)	Utilized LIBS for monitoring e-waste samples, significantly reducing the cost of gold recovery compared to market standards.	[187]

Trivedi's team[187] applied LIBS to monitor elemental compositions during laser ablation of electronic waste (E-waste) for precious metal recovery, achieving a gold recovery cost of only \$0.18/g—significantly lower than the market price of \$70–80/g—and reducing environmental hazards compared to traditional pyrometallurgical methods.

The literature reviewed above demonstrates that real-time LIBS monitoring has achieved significant advancements across various domains, including emerging manufacturing, transportation, underwater chemical dynamics, soil nutrients, clinical medicine, and precious metal recovery. Table 11 further organizes the technical characteristics of LIBS within these application scenarios and summarizes the innovative achievements of various research teams in terms of monitored substances and specific contributions.

CONCLUSION AND OUTLOOK

This study focuses on the application of LIBS technology in the field of real-time monitoring. In recent years, LIBS has made significant advances across industrial production, environmental monitoring, and laser processing. With its advantages of rapid analysis, high accuracy, and minimal sample preparation, LIBS demonstrates substantial application potential. In industrial contexts, precise and stable elemental analysis can effectively enhance production efficiency and product quality. In environmental monitoring, the ability to control and track pollutants provides reliable data support for environmental

optimization. In the monitoring of laser-based processes, the implementation of closed-loop feedback enables operational optimization and improved control.

Despite the broad application potential and inherent advantages of real-time LIBS monitoring, several challenges and deficiencies persist in practical implementations:

1. Multi-element monitoring is frequently compromised by matrix effects, where variations in sample properties lead to plasma instability and reduced experimental precision. The origins of matrix effects are manifold, arising from differences in physical properties—such as excitation potentials across various mineral classifications—or from self-absorption phenomena occurring at high elemental concentrations. Given that this issue is prevalent across numerous LIBS applications, the importance of developing methods for its suppression or elimination is self-evident.

2. Detection accuracy often degrades when analyzing irregular or complex surfaces, as well as non-solid media such as liquids and aerosols. This limitation is particularly pronounced in the monitoring of industrial raw materials or liquid phases.

3. Regarding ultra-trace element detection, LIBS still requires further refinements in precision to rival other high-sensitivity analytical techniques.

4. Data processing and analysis remain significant hurdles; ensuring that equipment can accurately identify and interpret vast quantities of spectral data presents a complex challenge.

Future research trends in LIBS are expected to focus on the following areas:

1. Further mitigation of matrix effects through multi-faceted approaches. From a hardware perspective, researchers can intervene at the physical stage of LIBS; for instance, Gaft [25] and several other teams have developed or tested double-pulse LIBS, which yields more uniform plasmas and thus reduces matrix interference. Alternatively, matrix effects can be minimized through parameter optimization, such as setting the laser energy within a specific "saturation zone" or selecting more effective wavelength bands. From a computational standpoint, predictive models and data processing methods can be optimized. For example, Zhang *et al.*[9] employed second-order nonlinear polynomials and internal standardization for model calibration in coal component monitoring, while Zhang's team[173] utilized a novel fusion method based on a dual-branch convolutional neural network with an attention module (DBAM-CNN) to process LIBS data. Chang's team[99] integrated LIBS with 3D scanning imaging technology. Furthermore, improving the physical detection environment is a viable strategy; Andrews's team[94] demonstrated the efficacy of performing LIBS analysis under Ar or He gas atmospheres. Future researchers in real-time monitoring may combine these strategies or develop additional methodologies to enhance stability and reliability.

2. Upgrading core LIBS instrumentation. Developing higher-frequency lasers and higher-resolution spectrometers is essential for improving intrinsic detection efficiency, precision, and sensitivity. Numerous teams[81,188–190] have applied femtosecond LIBS to real-time monitoring; compared to traditional nanosecond LIBS, its higher repetition rate significantly increases detection speed. Redoglio's[47] team developed a large depth-of-field system to address the poor detection stability caused by variations in the distance and angle between the plasma and the detector—a common issue in heterogeneous coal quality monitoring. Li *et al.*[35] utilized a Cassegrain telescope as the LIBS optical system, markedly improving the stability and accuracy of spectral data. Consequently, the continuous technological iteration of LIBS hardware represents a major future trend.

3. Integrating artificial intelligence (AI) and big data technologies: Leveraging AI-driven models and big data analytics for real-time spectral interpretation and automated processing will substantially enhance online analysis efficiency. Although studies combining LIBS-based real-time monitoring with AI remain limited, given the demonstrated capabilities and transformative potential of AI, it is anticipated that future research will increasingly adopt AI-driven methods for tasks such as automated elemental classification and data-assisted quantitative analysis.

4. Expanding LIBS applications across emerging fields: Owing to its capabilities for rapid, in situ, and multi-element online analysis, LIBS has already been adopted in diverse areas such as industrial manufacturing, advanced materials research, plasma physics, nuclear safety, laser processing quality control, resource exploration, environmental monitoring, and medical diagnostics. In the future, it is poised to extend into additional domains requiring real-time monitoring, including deep-sea exploration and investigations into the evolution of extremophile materials.

Beyond these highlighted applications, LIBS research continues to advance across many other disciplines. While it is not feasible to discuss every relevant study and outcome in detail here due to space constraints, the collective evidence underscores LIBS's substantial promise in real-time monitoring. Nonetheless, realizing its full potential will depend on addressing key obstacles, particularly its current limitations in analytical accuracy and the complexity of spectral data processing. With the rapid progress in laser technology, computational data processing, and its integration with fields such as materials science and plasma physics, LIBS is expected to continue evolving in multiple directions, ultimately becoming a mature and widely deployed tool for real-time monitoring.

ASSOCIATED CONTENT

The supporting information (Fig. S1 and Table S1) is available at https://www.at-spectrosc.com.

AUTHOR INFORMATION

Yun Tang is currently an associate professor at the School of Physics and Electronic Science, Hunan University of Science and Technology (HNUST)， Xiangtan, China. She received the Ph.D. degree in Electronic Science and Technology from Wuhan National Laboratory for Optoelectronics (WNLO) at Huazhong University of Science and Technology (HUST) of China in 2019. She has published more than 40 papers in the fields of laser-induced breakdown spectrometry developments.

Corresponding Authors

*Y. Tang

Email address: yuntang@hnust.edu.cn

Notes

The authors declare no competing financial interest.

Acknowledgments

This work was financially supported by the Natural Science Foundation of Hunan Province (2024JJ5166) and the Open Foundation of Hunan Province Key Laboratory of Intelligent Sensors and Advanced Sensor Materials (E22341).

REFERENCES

1. P. Acquafredda, *Phys. Sci. Rev.*, 2019, **4**. https://doi.org/10.1515/psr-2018-0171
2. A.A. Ammann, *J. Mass Spectrom.*, 2007, **42**, 419–427. https://doi.org/10.1002/jms.1206
3. S.R. Khan, B. Sharma, P.A. Chawla, and R. Bhatia, *Food Anal. Methods*, 2022, **15**, 666–688. https://doi.org/10.1007/s12161-021-02148-4
4. Atomic Absorption Spectroscopy, n.d.
5. S.J. Oks, M. Jalowski, M. Lechner, S. Mirschberger, M. Merklein, B. Vogel-Heuser, and K.M. Möslein, *Inf. Syst. Front.*, 2024, **26**, 1731–1772. https://doi.org/10.1007/s10796-022-10252-x
6. W. Yan, J. Wang, S. Lu, M. Zhou, and X. Peng, *Processes*, 2023, **11**, 369. https://doi.org/10.3390/pr11020369
7. H. Mahfoud, O. Moutaoukil, M. Toum Benchekroun, and A. Latif, in: M. Ezziyyani, J. Kacprzyk, V.E. Balas (Eds.), Int. Conf. Adv. Intell. Syst. Sustain. Dev. AI2SD2023, Springer Nature Switzerland, Cham, 2024, pp. 18–34. https://doi.org/10.1007/978-3-031-54288-6_3
8. L. X. Sun, W. Wang, P. Zhang, Y. Xin, L. F. Qi, *Metallurgical Analysis*, 2021, **41**, 58–67. https://doi.org/10.13228/j.boyuan.issn1000-7571.011612
9. L. Zhang, Z.-Y. Hu, W.-B. Yin, D. Huang, W.-G. Ma, L. Dong, H.-P. Wu, Z.-X. Li, L.-T. Xiao, and S.-T. Jia, *Front. Phys.*, 2012, **7**, 690–700. https://doi.org/10.1007/s11467-012-0259-7
10. X. Yu, Y. Li, X. Gu, J. Bao, H. Yang, and L. Sun, *Environ. Monit. Assess.*, 2014, **186**, 8969–8980. https://doi.org/10.1007/s10661-014-4058-1
11. Y. Zhang, T. Zhang, and H. Li, *Spectrochim. Acta Part B At. Spectrosc.*, 2021, **181**, 106218. https://doi.org/10.1016/j.sab.2021.106218
12. R.I. Ledesma, F.L. Palmieri, and J.W. Connell, in: Amsterdam, n.d.
13. J.D. Winefordner, I.B. Gornushkin, T. Correll, E. Gibb, B.W. Smith, and N. Omenetto, *J. Anal. At. Spectrom.*, 2004, **19**, 1061–1083. https://doi.org/10.1039/B400355C
14. B.E. Naes, S. Umpierrez, S. Ryland, C. Barnett, and J.R. Almirall, *Spectrochim. Acta Part B At. Spectrosc.*, 2008, **63**, 1145–1150. https://doi.org/10.1016/j.sab.2008.07.005
15. M. Yao, L. Huang, J. Zheng, S. Fan, and M. Liu, *Opt. Laser Technol.*, 2013, **52**, 70–74. https://doi.org/10.1016/j.optlastec.2013.04.005
16. K. Rawat, N. Sharma, and V.K. Singh, in: X-Ray Fluoresc. Biol. Sci., John Wiley & Sons, Ltd, 2022, pp. 1–20. https://doi.org/10.1002/9781119645719.ch1
17. C. Martinez-Lopez, O. Ovide, R. Corzo, Z. Andrews, J.R. Almirall, and T. Trejos, *Forensic Chem.*, 2022, **27**, 100384. https://doi.org/10.1016/j.forc.2021.100384
18. L. Jingwen, Y. Lixing, S. Li, and W. Cong, *Optoelectron. Lett.*, 2024, **20**, 116–121. https://doi.org/10.1007/s11801-024-3080-y
19. G. Hubmer, R. Kitzberger, and K. Mörwald, *Anal. Bioanal. Chem.*, 2006, **385**, 219–224. https://doi.org/10.1007/s00216-006-0321-9
20. M. Gaft, E. Dvir, H. Modiano, and U. Schone, *Spectrochim. Acta B*, 2008, **63**, 1177–1182. https://doi.org/10.1016/j.sab.2008.06.007
21. E. Xenogiannopoulou, C. Andreouli, and C. Stournaras, *J. Nano Res.*, 2009, **8**, 61–70. https://doi.org/10.4028/www.scientific.net/JNanoR.8.61
22. S. Mukherjee, in: S. Mukherjee (Ed.), Appl. Mineral. Appl. Ind. Environ., Springer Netherlands, Dordrecht, 2011, pp. 428–489. https://doi.org/10.1007/978-94-007-1162-4_17
23. J.D. Blacic, D.R. Pettit, and D.A. Cremers, Final Report on Feasibility of Real-Time Geochemical Analysis at Yucca Mountain, Nevada, Using LIBS Technology, Los Alamos National Lab. (LANL), Los Alamos, NM (United States), 1996. https://doi.org/10.2172/426979
24. M. Gaft, I. Sapir-Sofer, H. Modiano, and R. Stana, *Spectrochim. Acta B*, 2007, **62**, 1496–1503. https://doi.org/10.1016/j.sab.2007.10.041
25. M. Gaft, L. Nagli, I. Fasaki, M. Kompitsas, and G. Wilsch, *Spectrochim. Acta B*, 2009, **64**, 1098–1104. https://doi.org/10.1016/j.sab.2009.07.010
26. M. Gaft, L. Nagli, Y. Groisman, A. Barishnikov, M. Gaft, L. Nagli, Y. Groisman, and A. Barishnikov, *Appl. Spectrosc.*, 2014, **68**, 1004–1015. https://doi.org/10.1366/13-07382

27. D. L. Death, A. P. Cunningham, and L.J. Pollard, *Spectrochim. Acta B*, 2009, **64**, 1048–1058. https://doi.org/10.1016/j.sab.2009.07.017
28. X. Cheng, X. Yang, Z. Zhu, L. Guo, X. Li, Y. Lu, and X. Zeng, *Appl. Opt.*, 2017, **56**, 9144–9149. https://doi.org/10.1364/AO.56.009144
29. J. El Haddad, E.S. de Lima Filho, F. Vanier, A. Harhira, C. Padioleau, M. Sabsabi, G. Wilkie, and A. Blouin, *Miner. Eng.*, 2019, **134**, 281–290. https://doi.org/10.1016/j.mineng.2019.02.025
30. M. Wójcik, P. Brinkmann, R. Zdunek, D. Riebe, T. Beitz, S. Merk, K. Cieślik, D. Mory, A. Antończak, M. Wójcik, P. Brinkmann, R. Zdunek, D. Riebe, T. Beitz, S. Merk, K. Cieślik, D. Mory, and A. Antończak, *Sensors*, 2020, **20**. https://doi.org/10.3390/s20185152
31. R. Fuentes, D. Luarte, C. Sandoval, A.K. Myakalwar, J. Yáñez, and D. Sbarbaro, *Miner. Eng.*, 2021, **173**, 107193. https://doi.org/10.1016/j.mineng.2021.107193
32. J. Álvarez, M. Velásquez, C. Sandoval-Muñoz, R. del P. Castillo, C.Y. Bastidas, D. Luarte, D. Sbárbaro, D. Rammlmair, and J. Yáñez, *J. Anal. At. Spectrom.*, 2022, **37**, 1994–2004. https://doi.org/10.1039/D2JA00145D
33. K. Rifai, M.-C.M. Paradis, Z. Swierczek, F. Doucet, L. Özcan, A. Fayad, J. Li, F. Vidal, K. Rifai, M.-C.M. Paradis, Z. Swierczek, F. Doucet, L. Özcan, A. Fayad, J. Li, and F. Vidal, *Minerals*, 2020, **10**, 918. https://doi.org/10.3390/min10100918
34. J. Huang, W. Zhou, J. Zhu, Y. Zhang, and Y. Liu, *Microw. Opt. Technol. Lett.*, 2023, **65**, 1439–1447. https://doi.org/10.1002/mop.33622
35. A. Li, X. Zhang, X. Liu, Y. He, Y. Shan, H. Sun, W. Yi, and R. Liu, *Opt. Express*, 2023, **31**, 38728–38743. https://doi.org/10.1364/OE.505574
36. T. Chen, L. Sun, H. Yu, P. Zeng, and L. Qi, *Spectrochim. Acta B*, 2023, **210**, 106821. https://doi.org/10.1016/j.sab.2023.106821
37. F. Colao, R. Fantoni, V. Lazic, A. Paolini, F. Fabbri, G.G. Ori, L. Marinangeli, and A. Baliva, *Planet. Space Sci.*, 2004, **52**, 117–123. https://doi.org/10.1016/j.pss.2003.08.012
38. A. De Giacomo, M. Dell'Aglio, Z. Salajková, E. Vaníčková, D. Mele, and P. Dellino, *J. Volcanol. Geotherm. Res.*, 2022, **432**, 107675. https://doi.org/10.1016/j.jvolgeores.2022.107675
39. A. Taleb, M. Dell'Aglio, R. Gaudiuso, D. Mele, P. Dellino, and A. De Giacomo, *Appl. Spectrosc.*, 2024, **78**, 716-726. https://doi.org/10.1177/00037028241241076
40. D. Body, and B.L. Chadwick, *Spectrochim. Acta B*, 2001, **56**, 725–736. https://doi.org/10.1016/S0584-8547(01)00186-0
41. B.L. Chadwick, and D. Body, *Appl. Spectrosc.*, 2002, **56**, 70–74
42. M. Noda, Y. Deguchi, S. Iwasaki, and N. Yoshikawa, *Spectrochim. Acta B*, 2002, **57**, 701–709. https://doi.org/10.1016/S0584-8547(01)00403-7
43. M. Kurihara, K. Ikeda, Y. Izawa, Y. Deguchi, and H. Tarui, *Appl. Opt.*, 2003, **42**, 6159–6165. https://doi.org/10.1364/AO.42.006159
44. R. Gurjar, and P. D, Development of Real-Time Coal Monitoring Instrument, Radiation Monitoring Devices, Inc., Watertown, MA 02472-4699, 2010. https://doi.org/10.2172/981919
45. C.E. Romero, R.D. Saro, J. Craparo, A. Weisberg, R. Moreno, and Z. Yao, *Energy Fuels*, 2010, **24**, 510–517. https://doi.org/10.1021/ef900873w
46. L. Zhang, Y. Gong, Y. Li, X. Wang, J. Fan, L. Dong, W. Ma, W. Yin, and S. Jia, *Spectrochim. Acta B*, 2015, **113**, 167–173. https://doi.org/10.1016/j.sab.2015.09.021
47. D. Redoglio, E. Golinelli, S. Musazzi, U. Perini, and F. Barberis, *Spectrochim. Acta B*, 2016, **116**, 46–50. https://doi.org/10.1016/j.sab.2015.11.005
48. S. Legnaioli, B. Campanella, S. Pagnotta, F. Poggialini, and V. Palleschi, *Spectrochim. Acta B*, 2019, **155**, 123–126. https://doi.org/10.1016/j.sab.2019.03.012
49. Y. Ma, W. Zhang, Z. Xiong, H. Cui, Q. Li, R. Zhou, Y. Zhang, X. Li, X. Zeng, and Q. Li, *J. Anal. At. Spectrom.*, 2020, **35**, 1458–1463. https://doi.org/10.1039/C9JA00448C
50. K. Zhan, J. Chen, C. He, Z. Tang, Q. Li, K. Liu, C. Zhu, and X. Li, *J. Anal. At. Spectrom.*, 2021, **36**, 1210–1216. https://doi.org/10.1039/D1JA00047K
51. Q. Ni, Y. Zhu, W. Zhu, Y. He, and Z. Wang, *ACS Omega*, 2022, **7**, 9443–9451. https://doi.org/10.1021/acsomega.1c06752
52. Y. Dou, Q. Wang, S. Wang, X. Shu, M. Ni, and Y. Li, *Appl. Sci.*, 2023, **13**, 10049. https://doi.org/10.3390/app131810049
53. R. Liu, L. An, X. Zhang, X. Liu, and H. Sun, *J. Anal. At. Spectrom.*, 2025, **40**, 3274-3279. https://doi.org/10.1039/D5JA00011D
54. Z. Tian, X. Li, G. Wang, L. Zhang, J. Li, S. Wang, Y. Bai, W. Zhang, H. Yue, X. Ma, W. Yin, and S. Jia, *Plasma Sci. Technol.*, 2022, **24**, 084007. https://doi.org/10.1088/2058-6272/ac78ca
55. Z. Wang, Y. Deguchi, F. Shiou, J. Yan, and J. Liu, *ISIJ Int.*, 2016, **56**, 723–735. https://doi.org/10.2355/isijinternational.ISIJINT-2015-542
56. J. Gruber, J. Heitz, H. Strasser, D. Bäuerle, and N. Ramaseder, *Spectrochim. Acta B*, 2001, **56**, 685–693. https://doi.org/10.1016/S0584-8547(01)00182-3
57. J. Gruber, J. Heitz, N. Arnold, D. Bäuerle, N. Ramaseder, W. Meyer, J. Hochörtler, and F. Koch, *Appl. Spectrosc.*, 2004, **58**, 457–462. https://doi.org/10.1366/000370204773580310
58. J. Heitz, J. Gruber, N. Arnold, D. Bauerle, N. Ramaseder, W. Meyer, and J. Hochortler, in: XIV Int. Symp. Gas Flow Chem. Lasers High-Power Lasers, SPIE, 2003, pp. 588–595. https://doi.org/10.1117/12.515827
59. K. Chen, J. Lu, and J. Li, *Spectrosc. Spectr. Anal.*, 2011, **31**, 823–826. https://doi.org/10.3964/j.issn.1000-0593(2011)03-0823-04
60. L.X. Sun, Y. Xin, Z.B. Cong, Y. Li, and L.F. Qi, *Adv. Mater. Res.*, 2013, **694–697**, 1260–1266. https://doi.org/10.4028/www.scientific.net/AMR.694-697.1260
61. L. Sun, H. Yu, Z. Cong, Y. Xin, Y. Li, and L. Qi, *Spectrochim. Acta B*, 2015, **112**, 40–48. https://doi.org/10.1016/j.sab.2015.08.008
62. V. Sturm, R. Fleige, M. De Kanter, R. Leitner, K. Pilz, D. Fischer, G. Hubmer, and R. Noll, *Anal. Chem.*, 2014, **86**, 9687–9692. https://doi.org/10.1021/ac5022425
63. G. Lorenzetti, S. Legnaioli, E. Grifoni, S. Pagnotta, and V. Palleschi, *Spectrochim. Acta B*, 2015, **112**, 1–5. https://doi.org/10.1016/j.sab.2015.07.006
64. J. Ruiz, T. Delgado, L. M. Cabalín, and J. J. Laserna, *J. Anal. At. Spectrom.*, 2017, **32**, 1119–1128. https://doi.org/10.1039/C7JA00093F
65. L.M. Cabalín, T. Delgado, J. Ruiz, D. Mier, and J.J. Laserna, *Spectrochim. Acta B*, 2018, **146**, 93–100. https://doi.org/10.1016/j.sab.2018.05.001
66. Z. Wang, Y. Deguchi, F. Shiou, S. Tanaka, M. Cui, K. Rong, and J. Yan, *ISIJ Int.*, 2020, **60**, 971–978. https://doi.org/10.2355/isijinternational.ISIJINT-2019-317
67. M. J. Torkamany, E. Gholami, and S. Batebi, *Amirkabir J. Mech. Eng.*, 2024, **56**, 1275–1302. https://doi.org/10.22060/mej.2025.23511.7774
68. P.A. Sdvizhenskii, D.Yu. Karpenkov, A.V. Rogachevskaya, S.V. Volokhov, K.E. Galeru, D.V. Kuznetsov, and V.N. Lednev, *Opt. Laser Technol.*, 2025, **183**, 112378. https://doi.org/10.1016/j.optlastec.2024.112378

69. J. Magnes, *Alloys*, 2021, **9**, 705–747. https://doi.org/10.1016/j.jma.2021.04.001
70. B. Stojanovic, M. Bukvic, and I. Epler, *Appl. Eng. Lett. J. Eng. Appl. Sci.*, 2018, **3**, 52-62. https://doi.org/10.18485/aeletters.2018.3.2.2
71. R.D. Saro, A. Weisberg, and J. Craparo, 2005. https://doi.org/10.1021/ef900873w
72. R.D. Saro, In-Situ, Real-Time Measurement of Melt Constituents in the Aluminum, Glass, and Steel Industries, Energy Research Company, 2006. https://doi.org/10.2172/882367
73. Q. Zeng, C. Pan, C. Li, T. Fei, X. Ding, X. Du, and Q. Wang, *Spectrochim. Acta B*, 2018, **142**, 68–73. https://doi.org/10.1016/j.sab.2018.01.011
74. S.H. Gudmundsson, J. Matthiasson, B.M. Björnsson, H. Gudmundsson, and K. Leosson, *Spectrochim. Acta B*, 2019, **158**, 105646. https://doi.org/10.1016/j.sab.2019.105646
75. S.H. Gudmundsson, J. Matthiasson, and K. Leosson, in: A. Tomsett (Ed.), Light Met. 2020, Springer International Publishing, Cham, 2020, pp. 860–864. https://doi.org/10.1007/978-3-030-36408-3_114
76. Y. Xin, L.-X. Sun, Z.-J. Yang, P. Zeng, Z.-B. Cong, and L.-F. Qi, *Front. Phys.*, 2016, **11**, 115207. https://doi.org/10.1007/s11467-016-0619-9
77. E. Baril, L. St-Onge, M. Sabsabi, J. Lucas, M. Gagné, and J. Lucas, in: 2004, 16th world conference on NDT. https://www.ndt.net/article/wcndt2004/pdf/in-process_ndt-nde/679_sabsabi.pdf
78. A.K. Myakalwar, C. Sandoval, B. Sepúlveda, R. Fuentes, R. Parra, E. Balladares, A. Vásquez, D. Sbarbaro, and J. Yáñez, *Anal. Chim. Acta*, 2021, **1178**, 338805. https://doi.org/10.1016/j.aca.2021.338805
79. Y. Liu, M. Li, Z. An, T. Zhang, J. Liu, Y. Liang, H. Tang, J. Gong, D. Yan, Z. You, and H. Li, *Chin. J. Anal. Chem.*, 2024, **52**, 100450. https://doi.org/10.1016/j.cjac.2024.100450
80. J. Spencer, B. Squires, B. McWilliams, K. Cho, N.B. Dahotre, and A.A. Voevodin, *Surf. Coat. Technol.*, 2024, **494**, 131375. https://doi.org/10.1016/j.surfcoat.2024.131375
81. J. Liu, J. Wang, X. Li, H. Lin, T. Liu, B. Zhou, and X. He, *RSC Adv.*, 2025, **15**, 1549–1556. https://doi.org/10.1039/D4RA07007K
82. I. Kastelli, L. Mamica, and K. Lee, *Rev. Evol. Polit. Econ.*, 2023, **4**, 1–25. https://doi.org/10.1007/s43253-023-00100-2
83. F.J. Gomes da Silva, and R.M. Gouveia, in: F.J. Gomes da Silva, R.M. Gouveia (Eds.), Clean. Prod. Better Future, Springer International Publishing, Cham, 2020, pp. 33–75. https://doi.org/10.1007/978-3-030-23165-1_3
84. L. Alcorta, *Development*, 2015, **58**, 528–539. https://doi.org/10.1057/s41301-016-0057-6
85. F.-Y. Yueh, J.P. Singh, and Z. Hansheng, Encyclopedia of Analytical Chemistry: Applications, Theory and Instrumentation, 2006. https://doi.org/10.1002/9780470027318.a0708
86. D.W. Hahn, K.R. Hencken, and H.A. Johnsen, Performance Testing of a Laser-Induced Breakdown Spectroscopy (LIBS) Based Continuous Metal Emissions Monitor at a Pyrolytic Waste Treatment Facility, Sandia Labs., Livermore, CA (United States), 1997. https://doi.org/10.2172/552757
87. D.W. Hahn, W.L. Flower, and K.R. Hencken, *Appl. Spectrosc.*, 1997, **51**, 1836–1844. https://doi.org/10.1366/0003702971939659
88. H. Zhang, F.-Y. Yueh, and J.P. Singh, *Appl. Opt.*, 1999, **38**, 1459–1466. https://doi.org/10.1364/AO.38.001459
89. R. Kumar, A.K. Rai, D. Alamelu, and S.K. Aggarwal, *Environ. Monit. Assess.*, 2013, **185**, 171–180. https://doi.org/10.1007/s10661-012-2541-0
90. C. Dutouquet, G. Gallou, O. Le Bihan, J.B. Sirven, A. Dermigny, B. Torralba, and E. Frejafon, *Talanta*, 2014, **127**, 75–81. https://doi.org/10.1016/j.talanta.2014.03.063
91. J.A. Garcia, J.R.A. da Silva, and E.R. Pereira-Filho, *Microchem. J.*, 2021, **164**, 106007. https://doi.org/10.1016/j.microc.2021.106007
92. S. Tognana, C. D'Angelo, S. Montecinos, M. Pereyra, and W. Salgueiro, *Chemosphere*, 2022, **303**, 135168. https://doi.org/10.1016/j.chemosphere.2022.135168
93. H.B. Andrews, J. McFarlane, and K.G. Myhre, *Appl. Spectrosc.*, 2022, **76**, 988–997. https://doi.org/10.1177/00037028221088625
94. H.B. Andrews, Z.B. Kitzhaber, and J. McFarlane, *Spectrochim. Acta B*, 2025, **230**, 107237. https://doi.org/10.1016/j.sab.2025.107237
95. H.B. Andrews, and J. McFarlane, *Sensors*, 2023, **23**, 9797. https://doi.org/10.3390/s23249797
96. H.B. Andrews, Z.B. Kitzhaber, D. Orea, and J. McFarlane, *J. Am. Chem. Soc.*, 2025, **147**, 910–917. https://doi.org/10.1021/jacs.4c13684
97. A. Elhassan, M. Abdelhamid, M. Abdelkreem, and M. Abdel-Harith, in: Chennai, India, 2023, p. 070001. https://doi.org/10.1063/5.0119950
98. C.R. Bhatt, D. Hartzler, and D. McIntyre, *Appl. Phys. B*, 2023, **130**, 18. https://doi.org/10.1007/s00340-023-08156-y
99. C. Chang, F. Di Maio, R. Bheemireddy, P. Posthoorn, A.T. Gebremariam, and P. Rem, *Comput. Ind.*, 2025, **164**, 104196. https://doi.org/10.1016/j.compind.2024.104196
100. D. Capela, S. Pessanha, T. Lopes, R. Cavaco, J. Teixeira, M.F.S. Ferreira, P. Magalhães, P.A.S. Jorge, N.A. Silva, and D. Guimarães, *J. Hazard. Mater.*, 2025, **489**, 137493. https://doi.org/10.1016/j.jhazmat.2025.137493
101. Z. Zhou, W. Sun, J. Wu, H. Chen, F. Zhang, and S. Wang, *Processes*, 2023, **11**, 1445. https://doi.org/10.3390/pr11051445
102. X. Li, and Y. Guan, *Metals*, 2021, **11**, 790. https://doi.org/10.3390/met11050790
103. S. Klein, J. Hildenhagen, K. Dickmann, T. Stratoudaki, and V. Zafiropulos, *J. Cult. Herit.*, 2000, **1**, S287–S292. https://doi.org/10.1016/S1296-2074(00)00173-4
104. F.J. Fortes, L.M. Cabalín, and J.J. Laserna, *Spectrochim. Acta B*, 2008, **63**, 1191–1197. https://doi.org/10.1016/j.sab.2008.06.009
105. A. Khedr, V. Papadakis, P. Pouli, D. Anglos, and M.A. Harith, *Appl. Phys. B*, 2011, **105**, 485–492. https://doi.org/10.1007/s00340-011-4492-5
106. L. X. Sun, W. J. Wang, L. F. Qi, Y. Lu, H. C. Qiao, and W. Wang, *Chinese Journal of Lasers*, 2020, **47**, 299–308. https://www.researching.cn/zgjg/allissues
107. W. Wang, L. Sun, Y. Lu, L. Qi, W. Wang, and H. Qiao, *Opt. Laser Technol.*, 2022, **145**, 107481. https://doi.org/10.1016/j.optlastec.2021.107481
108. A.A. Voznesenskaya, D.S. Gusev, D.A. Kochuev, A.A. Polyakova, and K.A. Frolov, *J. Phys. Conf. Ser.*, 2022, **2316**, 012006. https://doi.org/10.1088/1742-6596/2316/1/012006
109. Y. Li, B. Qin, J. Zhao, J. Zhao, C. Zhou, Zhizhong. Liu, R. Wu, Q. Li, Y. Zhang, and Q. Dai, in: 2024 2nd Int. Conf. Signal Process. Intell. Comput. SPIC, 2024, pp. 90–94. https://doi.org/10.1109/SPIC62469.2024.10691461
110. Z. Lei, Q. Meng, X. Zhang, X. Li, C. Wang, and B. Zhao, *Materials*, 2025, **18**, 1843. https://doi.org/10.3390/ma18081843

111. Z. Xu, Y. Bai, J. Yan, X. Liu, and J. Yang, *Surf. Interfaces*, 2025, **56**, 105533. https://doi.org/10.1016/j.surfin.2024.105533

112. W. Li, X. Su, J. Gu, Y. Jin, J. Xu, and B. Guo, *Photonics*, 2023, **10**, 96. https://doi.org/10.3390/photonics10010096

113. J. Li, J. Yang, J. Liu, H. Chen, Y. Duan, and X. Pan, *Materials*, 2024, **17**, 2414. https://doi.org/10.3390/ma17102414

114. W. Yang, Z. Qian, Y. Cao, Y. Wei, C. Fu, T. Li, D. Lin, and S. Li, *J. Spectrosc.*, 2021, **2021**, 4614388. https://doi.org/10.1155/2021/4614388

115. D. Lin, W. Yang, Z. Qian, S. Li, Y. Hu, G. Li, and S. Zhang, *Appl. Opt.*, 2023, **62**, 2569–2576. https://doi.org/10.1364/AO.484404

116. S. Li, Y. Yang, S. Gao, D. Lin, G. Li, Y. Hu, and W. Yang, *Opt. Express*, 2024, **32**, 4122–4136. https://doi.org/10.1364/OE.511945

117. W. Yang, G. Li, Z. Qian, Y. Cao, D. Lin, S. Li, X. Zheng, D. Zhu, M. Xie, and Y. Yang, *Anal. Methods*, 2024, **16**, 4700–4709. https://doi.org/10.1039/D4AY00872C

118. Q. Zhou, G. Deng, Y. Chen, and S. Zhou, *Appl. Opt.*, 2019, **58**, 9421–9425. https://doi.org/10.1364/AO.58.009421

119. J. ShangGuan, Y. Tong, A. Yuan, X. Ren, J. Liu, H. Duan, Z. Lian, X. Hu, J. Ma, Z. Yang, and D. Wang, *J. Laser Appl.*, 2022, **34**, 022009. https://doi.org/10.2351/7.0000597

120. S. Choi, J. Choi, and C. Park, *Appl. Phys. B*, 2022, **129**, 8. https://doi.org/10.1007/s00340-022-07942-4

121. Y. Zhao, X. Zhuo, Y. Tong, J. Huang, S. Wang, W. Zhou, L. Chen, Y. Chen, and W. Shi, *J. Russ. LASER Res.*, 2024, **45**, 354–364. https://doi.org/10.1007/s10946-024-10221-6

122. T. Tong, J.G. Li, and J.P. Longtin, *Appl. Opt.*, 2004, **43**, 1971–1980. https://doi.org/10.1364/AO.43.001971

123. L. Song, W. Huang, X. Han, and J. Mazumder, *IEEE Trans. Ind. Electron.*, 2017, **64**, 633–642. https://doi.org/10.1109/TIE.2016.2608318

124. M. Jandaghi, P. Parvin, M.J. Torkamany, and J. Sabbaghzadeh, *J. Phys. -Appl. Phys.*, 2009, **42**, 205301. https://doi.org/10.1088/0022-3727/42/20/205301

125. M. Jandaghi, P. Parvin, M.J. Torkamany, and J. Sabbaghzadeh, *Phys. Procedia*, 2010, **5**, 107–114. https://doi.org/10.1016/j.phpro.2010.08.035

126. V.N. Lednev, P.A. Sdvizhenskii, M.Y. Grishin, A.Y. Stavertiy, R.S. Tretyakov, R.D. Asyutin, A.N. Fedorov, and S.M. Pershin, *Appl. Opt.*, 2021, **60**, 1144–1149. https://doi.org/10.1364/AO.411359

127. V.N. Lednev, P.A. Sdvizhenskii, M.Y. Grishin, A.Y. Stavertiy, R.S. Tretyakov, R.D. Asyutin, and S.M. Pershin, *Phys. Wave Phenom.*, 2021, **29**, 221–228. https://doi.org/10.3103/S1541308X21030092

128. N.A. Maslov, S.A. Konstantinov, and A.G. Malikov, *Russ. J. Nondestruct. Test.*, 2023, **59**, 736–742. https://doi.org/10.1134/S1061830923700444

129. L. Quackatz, I. Gornushkin, A. Griesche, T. Kannengiesser, K. Treutler, and V. Wesling, *Spectrochim. Acta B*, 2024, **214**, 106899. https://doi.org/10.1016/j.sab.2024.106899

130. H.J. Yoo, H. Kang, H. Kim, G. Lim, and S. Choi, 2026, . https://doi.org/10.2139/ssrn.6019577

131. S. Shangguan, J. Zhang, Z. Li, W. Shi, W. Wang, D. Qi, and H. Zheng, *Sci. China-Technol. Sci.*, 2024, **67**, 73–82. https://doi.org/10.1007/s11431-023-2499-0

132. H. Choi, A. Phoulady, P. Hoveida, N. May, S. Shahbazmohamadi, and P. Tavousi, *Plos One,* 2024, **19**, e0290761. https://doi.org/10.1371/journal.pone.0290761

133. I. Jang, J. Lee, and S. Jeong, *Int. J. Precis. Eng. Manuf.-Green Technol.*, 2025, **12**, 785–798. https://doi.org/10.1007/s40684-025-00715-2

134. B. Hettinger, V. Hohreiter, M. Swingle, and D.W. Hahn, *Appl. Spectrosc.*, 2006, **60**, 237–245. https://doi.org/10.1366/000370206776342544

135. R.S. Harmon, F.C.D. Lucia, C.A. Munson, A.W. Miziolek, and K.L. McNesby, in: Chem. Biol. Sens. Ind. Environ. Secur., SPIE, 2005, pp. 148–154. https://doi.org/10.1117/12.629925

136. T. Arfin, A.M. Pillai, N. Mathew, A. Tirpude, R. Bang, and P. Mondal, *Environ. Sci. Pollut. Res.*, 2023, **30**, 125347–125369. https://doi.org/10.1007/s11356-023-29652-w

137. J.E. Carranza, B.T. Fisher, G.D. Yoder, and D.W. Hahn, *Spectrochim. Acta B*, 2001, **56**, 851–864. https://doi.org/10.1016/S0584-8547(01)00183-5

138. G. Gallou, J.B. Sirven, C. Dutouquet, O.L. Bihan, and E. Frejafon, *Aerosol Sci. Technol.*, 2011, **45**, 918–926. https://doi.org/10.1080/02786826.2011.566899

139. P. Diwakar, P. Kulkarni, and M.E. Birch, *Aerosol Sci. Technol.*, 2012, **46**, 316–332. https://doi.org/10.1080/02786826.2011.625059

140. T. Tjärnhage, P.-Å. Gradmark, A. Larsson, A. Mohammed, L. Landström, E. Sagerfors, P. Jonsson, F. Kullander, and M. Andersson, *Opt. Commun.*, 2013, **296**, 106–108. https://doi.org/10.1016/j.optcom.2013.01.044

141. D. Girón, T. Delgado, J. Ruiz, L.M. Cabalín, and J.J. Laserna, *Measurement*, 2018, **115**, 1–10. https://doi.org/10.1016/j.measurement.2017.09.046

142. G. Kim, K. Kim, H. Maeng, H. Lee, and K. Park, *Aerosol Air Qual. Res.*, 2019, **19**, 455–460. https://doi.org/10.4209/aaqr.2018.08.0312

143. Y. Qu, Q. Zhang, W. Yin, Y. Hu, and Y. Liu, *Opt. Express*, 2019, **27**, A790–A799. https://doi.org/10.1364/OE.27.00A790

144. H. He, Z. Gao, Y. He, Q. Liu, X. Zhang, and B. Guo, in: A. Luo, Y. Feng, Z. Yang (Eds.), AOPC 2022 Opt. Spectrosc. Imaging, SPIE, Beijing, China, 2023, p. 1. https://doi.org/10.1117/12.2643868

145. E. Wan, Z. Sun, and Y. Liu, *Optik*, 2021, **245**, 167711. https://doi.org/10.1016/j.ijleo.2021.167711

146. E. Wan, Q. Zhang, L. Li, Q. Xie, X. Li, and Y. Liu, *Opt. Lasers Eng.*, 2024, **174**, 107974. https://doi.org/10.1016/j.optlaseng.2023.107974

147. C. Prüfert, T. Beitz, O. Reich, and H.-G. Löhmannsröben, *Spectrochim. Acta B*, 2022, **197**, 106527. https://doi.org/10.1016/j.sab.2022.106527

148. B. Han, J. Feng, D. Tian, Z. Chen, A. Iroshan, and Y. Liu, *Spectrochim. Acta B*, 2024, **217**, 106973. https://doi.org/10.1016/j.sab.2024.106973

149. N. Aizezi, Y. Ye, Z. Chen, and Y. Liu, *Spectrochim. Acta B*, 2025, **225**, 107124. https://doi.org/10.1016/j.sab.2025.107124

150. Y. Ye, N. Aizezi, J. Feng, B. Han, X. Li, Z. Su, L. Li, and Y. Liu, *Anal. Chem.*, 2025, **97**, 5554–5562. https://doi.org/10.1021/acs.analchem.4c05988

151. M. Huang, A. Iroshan, W. Gao, Z. Zhao, and Y. Liu, *J. Laser Appl.*, 2025, **37**, 022028. https://doi.org/10.2351/7.0001818

152. B.W. Smith, A Practical Laser Induced Breakdown Spectrometer for Real Time On- Line Monitoring of Aqueous Process Streams. Final Report, August 13, 1996--March 6, 1997, J. and D. Scientific, Inc., Gainesville, FL (United States), 1997. https://doi.org/10.2172/10201398

153. D.A. Hartzler, J.C. Jain, and D.L. McIntyre, *Sci. Rep.*, 2019, **9**, 4430. https://doi.org/10.1038/s41598-019-41025-3

154. L. Jiang, M. Sui, Y. Fan, H. Su, Y. Xue, and S. Zhong, *Spectrochim. Acta B*, 2021, **177**, 106065. https://doi.org/10.1016/j.sab.2021.106065

155. M. Sui, Y. Fan, L. Jiang, Y. Xue, J. Zhou, and S. Zhong, *Spectrochim. Acta B*, 2021, **180**, 106201. https://doi.org/10.1016/j.sab.2021.106201

156. T. Luo, W. Huang, R. Chen, F. Chen, J. Chen, Z. Hu, and J. Nie, *Chemosensors*, 2025, **13**. https://doi.org/10.3390/chemosensors13080271

157. Y. Xiong, W. Huang, J. Yang, J. Nie, and L. Guo, *J. Anal. At. Spectrom.*, 2025, **40**, 503–512. https://doi.org/10.1039/D4JA00381K

158. H.B. Andrews, Z.B. Kitzhaber, B.T. Manard, M.Z. Martin, and L.R. Sadergaski, *J. Anal. At. Spectrom.*, 2025, **40**, 689–699. https://doi.org/10.1039/D4JA00393D

159. G. LeCroy, Q. Yang, M. Raab, R. Gakhar, and A. Williams, 2025. https://doi.org/10.26434/chemrxiv-2025-5frjg

160. Y. Wang, H. Gao, J. Ye, J. Song, D. Wang, J. Han, G. Wang, B. Du, and L. Wang, *Photonics*, 2025, **12**. https://doi.org/10.3390/photonics12121186

161. Z. Wang, H. Ma, W. Huang, L. Guo, and W. Cheng, *J. Anal. At. Spectrom.*, 2025. https://doi.org/10.1039/d5ja00353a

162. M. Dell'Aglio, R. Gaudiuso, G.S. Senesi, A. De Giacomo, C. Zaccone, T.M. Miano, and O. De Pascale, *J. Environ. Monit. JEM*, 2011, **13**, 1422–1426. https://doi.org/10.1039/c0em00780c

163. A. Ismaël, B. Bousquet, K.M.-L. Pierrès, G. Travaillé, L. Canioni, and S. Roy, *Appl. Spectrosc.*, 2011, **65**, 467–473

164. D. Meng, N. Zhao, Y. Wang, M. Ma, L. Fang, Y. Gu, Y. Jia, and J. Liu, *Spectrochim. Acta B*, 2017, **137**, 39–45. https://doi.org/10.1016/j.sab.2017.09.011

165. A. Li, X. Chuai, Y. Liu, L. Qiu, H. Cui, and W. Zhao, *Spectrochim. Acta B*, 2024, **216**, 106931. https://doi.org/10.1016/j.sab.2024.106931

166. S. Li, Q. Zheng, X. Liu, P. Liu, and L. Yu, *Molecules*, 2024, **29**, 3699. https://doi.org/10.3390/molecules29153699

167. X. Fu, Y. Gou, G. Li, S. Zhao, S. Ma, and C. Zhao, *Microchem. J.*, 2024, **204**, 110922. https://doi.org/10.1016/j.microc.2024.110922

168. X. Li, R. Chen, F. Liu, Z. You, J. Huang, J. Peng, and G. Li, *Comput. Electron. Agric.*, 2025, **229**, 109831. https://doi.org/10.1016/j.compag.2024.109831

169. Y. Gou, X. Fu, J. Zhang, J. Jiang, Y. Huang, S. Ma, C. Zhao, and G. Li, *J. Hazard. Mater.*, 2025, **487**, 137291. https://doi.org/10.1016/j.jhazmat.2025.137291

170. B. Han, W. Gao, J. Feng, A. Iroshan, J. Yang, G. Chen, Y. Zhang, N. Aizezi, and Y. Liu, *J. Hazard. Mater.*, 2025, **496**, 139284. https://doi.org/10.1016/j.jhazmat.2025.139284

171. F. Ferioli, P.V. Puzinauskas, and S.G. Buckley, *Appl. Spectrosc.*, 2003, **57**, 1183-1189. https://doi.org/10.1366/00037020360696071

172. L. Zhang, W. Yin, L. Dong, W. Ma, L. Xiao, and S. Jia, *IEEE Photonics J.*, 2017, **9**, 1–10. https://doi.org/10.1109/JPHOT.2017.2741066

173. C. Zhang, W. Song, Y. Lyu, Z. Liu, X. Gao, Z. Hou, and Z. Wang, *Anal. Chim. Acta*, 2025, **1351**, 343899. https://doi.org/10.1016/j.aca.2025.343899

174. J. Cheng, and M. Tong, *Eng. Proc.*, 2025, **89**, 22. https://doi.org/10.3390/engproc2025089022

175. H. Dong, X. Huang, L. Wadle, L. Trinh, P. Li, J.-F. Silvain, B. Cui, and Y. Lu, *J. Anal. At. Spectrom.*, 2025, **40**, 1249–1257. https://doi.org/10.1039/D4JA00437J

176. T. Amodeo, C. Dutouquet, F. Tenegal, B. Guizard, H. Maskrot, O. Le Bihan, and E. Fréjafon, *Spectrochim. Acta B*, 2008, **63**, 1183–1190. https://doi.org/10.1016/j.sab.2008.09.005

177. T. Amodeo, *Spectrochim. Acta Part B At. Spectrosc.*, 2009, **64**, 1141–1152. https://doi.org/10.1016/j.sab.2009.07.031

178. C. Alvarez-Llamas, N. Herlin-Boime, J.-B. Sirven, and O. Sublemontier, *Spectrochim. Acta B*, 2025, **225**, 107122. https://doi.org/10.1016/j.sab.2025.107122

179. X. Jiang, G. Sergienko, B. Schweer, N. Gierse, M. Hubeny, A. Kreter, S. Brezinsek, and Ch. Linsmeier, *Nucl. Mater. Energy*, 2017, **12**, 1224–1230. https://doi.org/10.1016/j.nme.2016.11.021

180. J. Cuñat, *Anal. Chim. Acta*, 2009, **633**, 38–42. https://doi.org/10.1016/j.aca.2008.11.045

181. C.L. Goueguel, J.C. Jain, D.L. McIntyre, C.G. Carson, and H.M. Edenborn, *J. Anal. At. Spectrom.*, 2016, **31**, 1374–1380. https://doi.org/10.1039/C6JA00086J

182. D. Lim, K. Keerthi, S. Perumbilavil, C.S. Suchand Sandeep, M.M. Antony, and M.V. Matham, *Chem. Biol. Technol. Agric.*, 2024, **11**, 111. https://doi.org/10.1186/s40538-024-00641-6

183. K. K, M.M. Antony, S. Perumbilavil, and M.V. Matham, in: Remote Sens. Agric. Ecosyst. Hydrol. XXVI, SPIE, 2024, pp. 245–248. https://doi.org/10.1117/12.3033822

184. Y. Li, Z. Shi, L. Jiao, N. Liu, Z. Xing, S. Ma, H. Tian, and D. Dong, 2025. https://doi.org/10.2139/ssrn.5288622

185. B. Zhang, Q. Zhang, Z. Yue, C. Sun, F. Ding, and J. Yu, *Spectrochim. Acta B*, 2025, **224**, 107107. https://doi.org/10.1016/j.sab.2024.107107

186. R. Nakanishi, M. Saeki, and H. Ohba, *J. Anal. At. Spectrom.*, 2025, **40**, 1185–1191. https://doi.org/10.1039/D4JA00467A

187. A. Trivedi, M. Khetri, A. Surampudi, and M.C. Gupta, *ACS Omega*, 2025, **10**, 26033–26040. https://doi.org/10.1021/acsomega.5c02781

188. A. Santagata, R. Teghil, G. Albano, D. Spera, P. Villani, A. De Bonis, G.P. Parisi, and A. Galasso, *Appl. Surf. Sci.*, 2007, **254**, 863–867. https://doi.org/10.1016/j.apsusc.2007.07.203

189. W. Wessel, A. Brueckner-Foit, J. Mildner, L. Englert, L. Haag, A. Horn, M. Wollenhaupt, and T. Baumert, *Eng. Fract. Mech.*, 2010, **77**, 1874–1883. https://doi.org/10.1016/j.engfracmech.2010.03.020

190. Y. Chen, Y. Jiang, J. Han, A. Chen, and M. Jin, *Opt. Lett.*, 2024, **49**, 3106–3109. https://doi.org/10.1364/OL.526093